DANMARKS OG GRØNLANDS GEOLOGISKE UNDERSØGELSE **RAPPORT 2024/10**

Analysis of the applicability of cuttings samples to test seal integrity, examples from the Triassic to Jurassic interval in 8 wells in Eastern Denmark

Niels H. Schovsbo & Henrik Ingermann Petersen

GEOLOGICAL SURVEY OF DENMARK AND GREENLAND
DANISH MINISTRY OF CLIMATE, ENERGY AND UTILITIES

G E U S

DANMARKS OG GRØNLANDS GEOLOGISKE UNDERSØGELSE **RAPPORT 2024/10**

Analysis of the applicability of cuttings samples to test seal integrity, examples from the Triassic to Jurassic interval in 8 wells in Eastern Denmark

Niels H. Schovsbo & Henrik Ingermann Petersen

GEOLOGICAL SURVEY OF DENMARK AND GREENLAND
DANISH MINISTRY OF CLIMATE, ENERGY AND UTILITIES

G E U S

Summary

The Danish subsurface has a high technical CO_2 storage potential with multiple large structures that are currently under investigation as CO_2 storage sites following the recent opening of the CO_2 licencing round onshore Denmark. Within the structures two main reservoir-seal pairs are investigated namely the Bunter Sandstone sealed by the Ørslev and Falster Formations, and the Gassum Formation sealed by the Fjerritslev Formation. To evaluate the seal integrity direct measurements and tests to gauge the rock properties are needed. In Denmark, the onshore wells were mainly drilled in the 1950-1980'ies and many of the old wells have no wire-line log data or very poor data when compared to modern standards. In addition, cores of the seal section were rarely taken and the only source of material for full formation evaluation of the seal integrity are in most cases cuttings samples. This report focuses on the applicability of cuttings samples to test seal integrity and is based on analyses of cuttings samples from the wells Gassum-1, Fjerritslev-2, J-1X, Vedsted-1, Rønde-1, Søllested-1, Nøvling-1 and Vinding-1.

Our cuttings analyses include photographing, conducting Handheld X-Ray Fluorescence (HH-XRF) measurements, determining the Total Organic Carbon (TOC, wt%), Total Carbon (TC, wt%) and Total Sulphur (TS, wt%) contents, and conducting pyrolysis (Hawk instrument) following the Rock-Eval method. Of the studied wells the Søllested-1 and Vinding-1 wells were not measured with HH-XRF due to insufficient material.

The first reservoir-seal pair includes the Lower – Mid Triassic Bunter Sandstone, Ørslev, and Falster Formations. These formations are distinct in their geological characteristics, predominantly characterized by terrestrial and evaporitic depositional settings. The second reservoir-seal pair encompasses the Upper Triassic – Lower Jurassic Gassum and Lower Jurassic Fjerritslev Formations deposited in humid fluvial to fully marine conditions. The two reservoir-seal pairs are clearly delineated by the chemical analysis and provides invaluable insights into the geological history and potential applicability of these formations for CCS, helping to make knowledge-based decisions for further sampling and testing of the seal integrity and capacity.

Cuttings quality

The lithologies of the cuttings from the Bunter Sandstone Formation are fairly uniform, likely due to the presence of thicker sand layers and a high net-to-gross reservoir ratio. As a result, the analysis of these samples is more likely to accurately represent the sandstone's composition. The cuttings from the Ørslev and Falster formations appear quite uniform, suggesting they may represent the average composition of the mudstone.

The lithologies of the cutting samples from the Gassum Formation display a varied composition, featuring both sand and interbedded muddy and cemented beds. This variety suggests that samples purely representing the Gassum sandstone have not been successfully isolated in the bulk cuttings analysis and/or that the Gassum Fm is heterolithic in the investigated interval - which is quite common. The Fjerritslev Formation is predominantly characterised by greenish to dark grey mudstone lithologies. However, in certain intervals, quartz grains and reddish carbonate fragments are observed, indicating the presence of interbedded sandstone and carbonate concretions within the formation.

For the oldest wells studied, Søllested-1, Vinding-1 and Gassum-1, the cuttings were of low abundance and seemingly poor quality, dominated by rock fragments of various colours. This led to the decision not to analyse by HH-XRF Søllested-1 and Vinding-1 due to the questionable representativeness of the samples.

We note a tendency for the cuttings being less radiogenic than expected based on *in-situ* wireline measurements of the formation. The cause for this is not fully understood but may reflect a high proportion of soft clay (smectitic?) and organic material that has been preferentially lost during the preparation in laboratory and/or handling at drill site. Further studies on this are recommended to be conducted involving re-sampling of wet cuttings and re-design of cleaning procedure to avoid preferential loss of soft clay. We thus recommend only to used cuttings data for

the parts of the formation where the cuttings radioactivity match the expected as a source of information to evaluate the seal and reservoir properties. Also, careful consideration of the cutting size fraction needs to be made in order to reduce the lithological fractionation within the different size fractions.

Ørslev and Falster seals: The formations are analysed only in the Rødby-1 and Søllested-1 wells. The formations displays a unique composition compared to younger formations. This sequence is characterized by sections rich in anhydrite and limestone, notably lacking pyrite. They have a more siliceous nature with a high silicon to aluminium (Si/Al) ratio than seen in younger formations. This ratio is indicative of a low clay content and suggests a relative high silt / sand content. The absence of pyrite, coupled with the presence of anhydrite, aligns well with the known depositional environment for these formations, which was predominantly terrestrial and oxidizing, with features formed under evaporitic conditions (Ørslev). The Falster Formation are dominantly composed by limestone and anhydrite as reflected by high Ca and S content. Proxies for siliciclastic indicate low content. The composition agrees with the current interpretation of a terrestrial and evaporitic depositional environment. Both formations have very low TOC contents.

Fjerritslev seal: The formation is studied in the Gassum-1, Fjerrislev-2, Vedsted-1, J-1X, and Nøvling-1 wells and show a consistent geochemical characteristic that are largely similar between the wells. A notable feature is the abundant presence of pyrite, which aligns well with a marine depositional environment. The TOC content is generally <2 wt% with the highest numbers occurring in the upper part of the formation (F-III and F-IV members).
No significant variations were observed in the potassium to aluminium (K/Al) ratio across these wells, suggesting a broadly similar range in shale (mudstone) (V_{shale}) content. The clay content is estimated to be highest in the lower to middle Fjerritslev Formation, potentially reaching 50% clay content, based on few data from the Vedsted-1 well available from the literature. According to the classification by Folk et al. (1970), the most clay-rich part of the Fjerritslev Formation can be classified as a mudstone. The stratigraphic trend shows a notably upward increase in carbonate content peaking in the top part of the Fjerritslev Formation (F-III and F-IV members).

Bunter Sandstone versus the Gassum Sandstone Reservoir
Cuttings from the Bunter Sandstone and Gassum reservoir exhibit distinctly different compositions. The Bunter Sandstone is characterized by a low Al/K ratio, a higher Si/Al ratio in comparison to cuttings from the Gassum Formation. These geochemical distinctions could be attributed to a higher content of potassium feldspar and carbonate cement in the Bunter Sandstone relative to the Gassum Formation as also noted by Weibel et al. (2017). For petrophysical models the difference mineralogy must be taken into consideration when the clay content is evaluated from the Gamma Ray (GR) curve.

Table of Contents

1. Introduction

Cuttings samples from the Triassic–Jurassic interval have been studied in eight wells across eastern Denmark as part of a broader effort to gather regional data on seal characteristics of potential CO_2 storage sites. The analysis encompassed the determination of Total Organic Carbon (TOC, wt%) content and thermal maturity, the use of Handheld XRF (HH-XRF) for elemental composition assessment, and photographic documentation to describe lithologies. These data are crucial for evaluating the quality of both reservoir and seal, representing initial yet significant steps in an extensive workflow that aims to culminate in a comprehensive assessments of seal integrity and capacity, and reservoir compatibility concerning CO_2 storage, as outlined by Schovsbo et al. (2023).

Initiated in Q3 2022, this study forms a part of the CCUS 2020–2024 initiative at GEUS, which focuses on the regional screening of suitable CO_2 storage sites in Denmark. The findings from this study are instrumental in contributing to the site-specific evaluations of potential storage locations, as detailed in further documentation by GEUS for the Rødby, Gassum and Lisa structures reported elsewhere. The recommendations provided in these reports based on data evaluation have been repeated in this report for consistency.

The wells included in this study are Gassum-1, Fjerritslev-2, J-1X, Vedsted-1, Rønde-1, Nøvling-1, Søllested-1, and Vinding-1, as illustrated in Figure 1. This selection of wells provides a comprehensive overview of the geological variations and potential CO_2 storage capacities within the region. The stratigraphy of the wells is evaluated from the compilation of lithostratigraphic tops in deep Danish exploration wells[1] and follows the generalised nomenclature c.f. Figure 2.

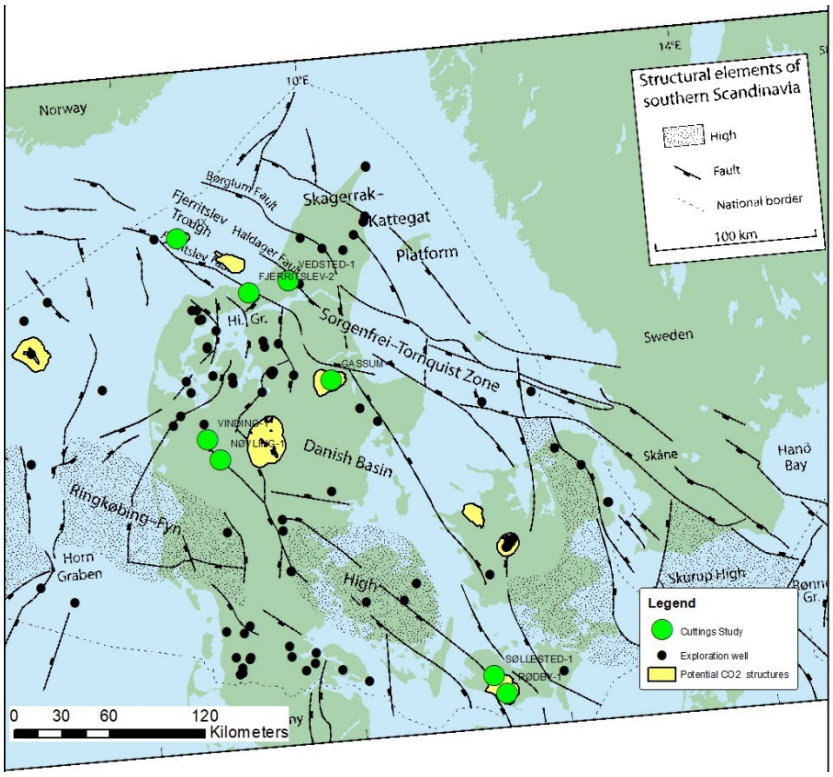

Figure 1 Location of studied wells and selected potential structures in eastern Denmark. Onshore structures were included in the recent CO_2 licence round (closed 24th January 2024). Structural map is from Nielsen (2003).

[1] GEUS, 2022, "Formation tops for deep exploration wells drilled in Denmark, v. 1.5", GEUS Dataverse, V2.

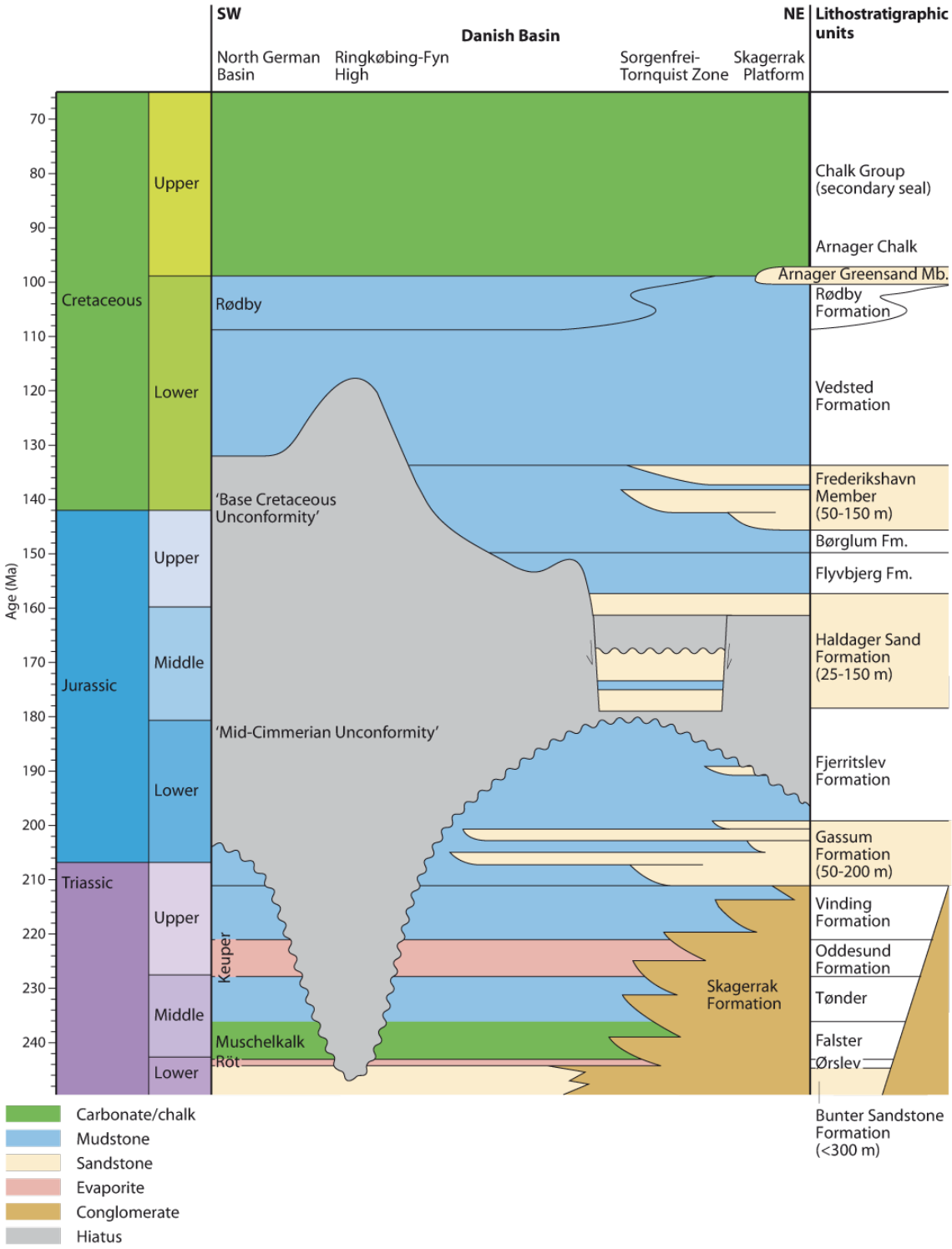

Figure 2 Stratigraphy of the studied area. From the Petroleum Geological Atlas of the Southern Permian Basin Atlas (Doornenbal and Stevenson, 2010).

2. Workflow

The wells and cuttings depths were picked as a supplement to those studied by Petersen et al. (2008) giving emphasis on stratigraphical and regional coverage.

The applied analysis workflow was (see also Figure 3):

1. Examination of existing washed and cleaned cuttings samples (dried cuttings): The primary focus was on existing dried cuttings samples. We aimed for approximately 10 grams of the 1–4 mm fraction. Due to time limitation, however, no additional sampling was undertaken from the "wet" unwashed and unprocessed cuttings samples.

2. Washing and sieving: Samples were washed with tap water and passed through sieves, separating them into the size fractions: less than 1 mm, 1–4 mm, and greater than 4 mm. The samples were then dried in an oven at 60°C. This was done in the Laboratory for Organic Carbon (LOK) at GEUS following standard procedures.

3. Photography of samples: The 1-4 mm fraction of each sample was photographed using a specialized setup at the Department of Mineral Resources and Mapping at GEUS to provide a visual documentation and a basis for further image analysis.

4. Crushing to rock powder: Approximately 4–6 grams of the 1–4 mm size fraction of each sample was crushed into rock powder (below 250 µm) using agate swing mills. This step was essential for homogenizing the sample for subsequent bulk rock analyses. This was done in the Laboratory for Organic Carbon (LOK) at GEUS following standard procedures.

5. Measurement of elemental composition: The powder was mounted in sample holder and measured using a Nithon XL3t GOLDD+ devise that provide Handheld X-Ray Fluorescence (HH-XRF) measurements at the Core Laboratory at GEUS.

6. TOC and TC/TS determinations, and Hawk pyrolysis using the Rock-Eval method: Total Organic Carbon (TOC, wt%) and TC/TS (wt%) determinations, and Rock-Eval type pyrolysis were performed on the rock powder in the Laboratory for Organic Carbon (LOK) at GEUS following standard procedures.

The workflow was designed to maximize the data gathering while minimising the cost and time consumption, and at the same time provide insights into the composition, lithology, and thermal maturity that is all key elements in a seal capacity assessment (Figure 3). The data gathered thus may serves as basis for selecting samples for more costly samples such as high-pressure Hg injection data (MICP), mineralogical (XRD) analysis of bulk and clay fraction, specific surface area determinations, and petrographical studies to determine organic matter distribution, rock fabric and grainsizes in later studies (Figure 3). See Schovsbo et al. (2022, 2023) for more extended workflow description proposed to evaluate seal integrity and capacity for potential CCS storage sites.

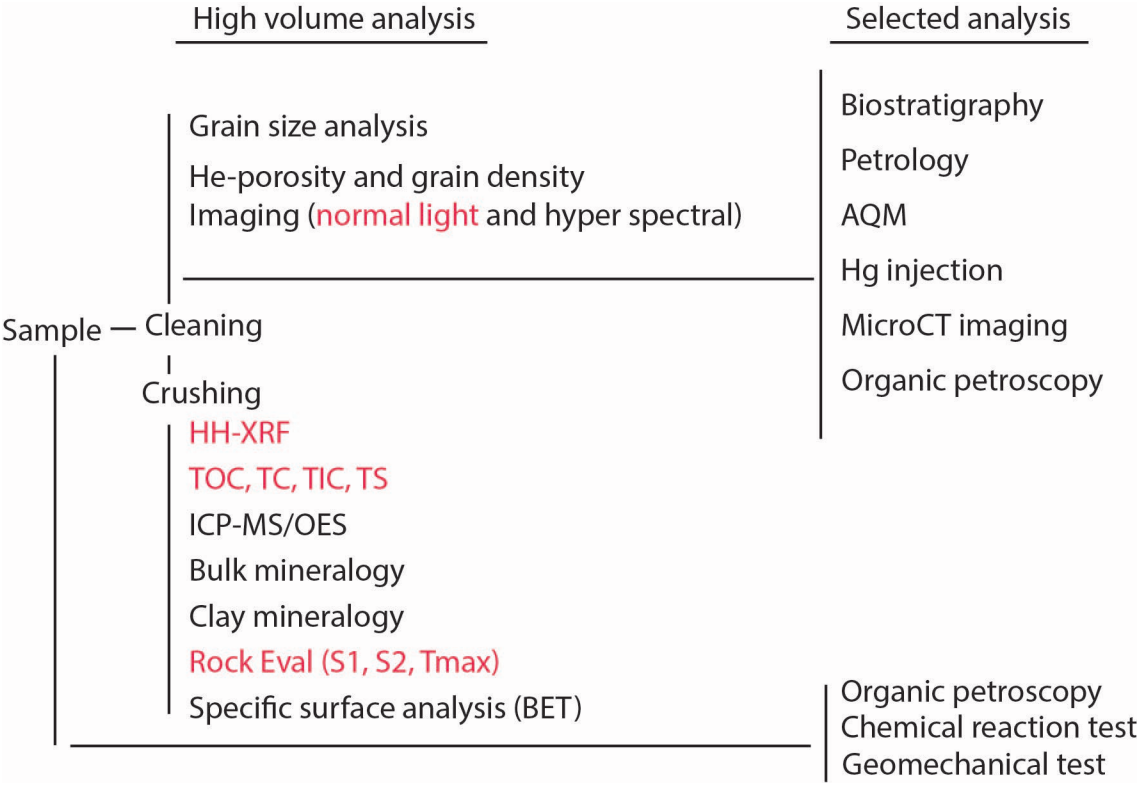

Figure 3 Workflow for seal and reservoir characterisation. In red are methods applied here. Based on Schovsbo et al. (2022, 2023) and this work.

3. Methods

3.1 Preparation

The cuttings were collected from the pre-prepared dried fraction. All samples underwent re-washing with tap water to eliminate any visible signs of contamination from drilling mud. As all wells involved in this study were drilled using water-based mud systems, cleaning by organic solvent extraction was not required. The sieving of samples was done by washing with tap water and passing through sieves, separating them into the size fractions: less than 1 mm, 1–4 mm, and greater than 4 mm. The sample fractions were then dried in an oven at temperatures below 60°C. The temperature was selected to prevent alteration by not heating the samples higher than what they had experienced during the geological history.

For powder, approximately 6 g of the 1–4 mm size fraction was ground to a particle size below 250 µm in an agate swing mill. Choosing the 1–4 mm size fraction is a standard within the LOK laboratory and supposedly minimize the influence of cavings, which are typically larger and more irregular in shape. The purpose behind grinding the cuttings was to ensure thorough mixing and homogenization of the sample material before conducting Handheld X-ray Fluorescence (HH-XRF), TOC determination and Hawk pyrolysis.

3.2 Cuttings images

Photographs of the cleaned cutting fraction, specifically the 1–4 mm size fraction, were taken using normal light. A fixed setup using a Canon EDX Mark II camera was used. No colour calibration was made. The images were initially captured in RAW (CR2) format and subsequently converted to the JPEG file format for ease of use and distribution.

3.3 HH-XRF

Measurements were conducted using a Nithon XL3t GOLDD+ device at the GEUS Core Analysis Laboratory (c.f. Schovsbo et al., 2018) (Figure 4). This device, equipped with a silver (Ag) anode, operates at voltage ranges from 6 to 50 kV and currents up to 200 µA, providing semi-quantitative elemental concentrations. The measurement area of the device is approximately 5 mm in diameter, and each measuring point was assessed for 2 to 2½ minutes using the 'test all geo filter', which conducts dual measurements on both low and high filters.

The analyses were performed on tablets made from the powdered material. Prior to the main analysis, preliminary tests were conducted to determine the minimum amount of powder required for the Nithon XL3t GOLDD+ to achieve stable readings on its 'balance indicator', ensuring that the readings were unaffected by the quantity of sample material. These tests involved incrementally increasing the sample amount from 0.5 grams to 6 grams using three different samples. The pellets were compacted by hand. It was determined that a minimum of 2 grams, and preferably at least 4 grams of material was needed to ensure stable and reliable measurements (see Section 4.2).

During analysis, the weight of the powder for each sample was recorded and samples weighing less than 2.0 grams were excluded before starting the data analysis to maintain consistency and accuracy. Furthermore, samples exhibiting low balance readings were also removed from the dataset prior to the analysis of data to ensure the integrity and reliability of the results.

Figure 4 The Nithon XL3t GOLDD+ in a fixed analytical set-up at GEUS for measuring powdered samples.

Quality and reliability of the HH-XRF data were ensured through measurements of both in-house and certified powder samples. The Nithon XL3t GOLDD+ reliability and stability have been well-established, especially when matrix effects are minimized by comparing with reference samples of a similar matrix, as noted in Schovsbo et al. (2018). To calibrate and validate the Nithon XL3t GOLDD+ readings, certified standards from the Canadian and United States Geological Surveys such as 180-646 (CCRMP Till-4PP), 180-647 (SiO_2 99.995% PP), 180-649 (NIST 2709a PP), 180-661 (RCRApp 1000Ba 500Ag, As, Cd, Cr, Pb, Se), 180-673 (QC USGS SAR-M), and $CaCO_3$ (GEUS internal standard from analytical pure substance) were measured. See Appendix A for details of analysis.

Additionally, a set of eleven in-house lower Paleozoic shale samples, previously utilized by Schovsbo et al. (2018), were measured. Efforts are currently underway to measured additional interval standards from Cenozoic mudstones in the Danish area. Analysis of representative Lark Formation mudstone (c.f. Schovsbo et al., 2022) was thus made within the sample series to facilitate a correction to ICP-MS/OES determined element concentration. Conversion tables from NHH-XRF to ICP-MS/OES determined elements are presented in Appendix B. However, it is important to note that the HH-XRF elemental concentrations reported herein represent uncorrected determinations. The corrected data will be presented in later publications.

To further enhance the analysis, a Sum Gamma Ray API value (SGR) was calculated for each sample to compare with Gamma Ray (GR) wireline log API readings if this were recorded in the well.

The SGR calculation followed the formula:

$$SGR\ [API] = 19.6 \times K\ [\%] + 8.1 \times U\ [ppm] + 4.0 \times Th\ [ppm] \quad \text{(Eq 1)}$$

It is important to acknowledge, however, that for most samples, the U levels are below the HH-XRF detection limit, typically between 5–8 ppm. Therefore, in intervals where U contributes to the natural radioactivity level, this will not be fully reflected in the SGR calculation. As a result, the SGR values will be lower than the actual radioactive levels present in the samples and should rather be termed Clean Gamma Ray (CGR) to indicate that it is only the K and Th contribution to the API response that is reported.

We have here made an interpretation of the likely range of SGR in the sample where the concentration was below detection limit for U, Th and K. In these cases, the level of error of detection is used as the measure for the elements. The elements are labelled K_max, U_max and Th_max and were used to determine the SGR_max:

SGR_max [API] = 19.6 × K_max [%] + 8.1 × U_max [ppm] + 4.0 × Th_max [ppm]. (Eq 2)

The SGR_max is thus a measure of the API values that could exist given that that all elements were measured at least above the level of detection.

We note that a calibration of HH-XRF data to ICPMS/OES date has not yet been presented and thus the calculated API values will likely change in future reporting. Also no conversion of the weight-based SGR measurements to the volume-based measurements reflected by the GR tool by taking in the effect of porosity is made which also will impact the comparison.

3.4 TOC determinations

A LECO CS-200 induction furnace was used to determine the TOC (Total Organic Carbon), TC (Total Carbon) and TS (Total Sulphur) content. For determination of TC and TS 50 mg of the grounded sample (<250 µm) was used. TOC was determined after removal of carbonate-bond carbon by HCl treatment, and a total of 300 mg was pyrolyzed. The samples were also pyrolyzed in a Hawk Pyrolysis instrument (Wildcat Technologies), using the standard Rock-Eval 6 method. The method is a programmed temperature, anhydrous open pyrolysis method, which is widely used for analyzing the organic matter in sedimentary rocks (Bordenave et al., 1993; Lafargue et al., 1998). The standard program starts with 3 minutes of isothermal flash pyrolysis at 300 °C, followed by ramp heating carried out with a heating rate of 25 °C/min until a maximum temperature of 650 °C. During the pyrolysis the amount of free hydrocarbons (HC) in the sample (S1; mg HC/g rock) and the remaining HC generation potential of the kerogen (S2; mg HC/g rock) are measured by the flame ionization detector (FID; mv). The TOC content and the S2 yields are used to calculate the Hydrogen Index (HI; mg HC/g TOC). The temperature at maximum S2 generation is recorded as T_{max}, which is maturity dependent.

4. Results

Standards

Schovsbo et al. (2018) demonstrated a correlation between HH-XRF analyses and those performed using ICP-MS/OES. However, they did not present a systematic analysis of the reproducibility of standards analysed sequentially while operating the Nithon XL3t GOLDD+ device.

Figures 5 and 6 illustrate the Si and Ca measurements for four selected standards conducted over the specified time interval covering the analysis for the cuttings reported here (note that cuttings were not analysed for all days were standard were measured). Additionally, Table 1 provides key statistical data on these standards. A comprehensive analysis of the data is included in Appendix A.

The analysis of these standards suggests a consistency in the analytical data, as evidenced by Figures 5 and 6, indicating no significant drift within the analysis time span. Furthermore, the routine practice of beginning and concluding daily analysis sequences with standard measurements has not shown any notable differences between initial and last sample runs. This consistency in the results reinforces the reliability of the HH-XRF device used for sequential analyses.

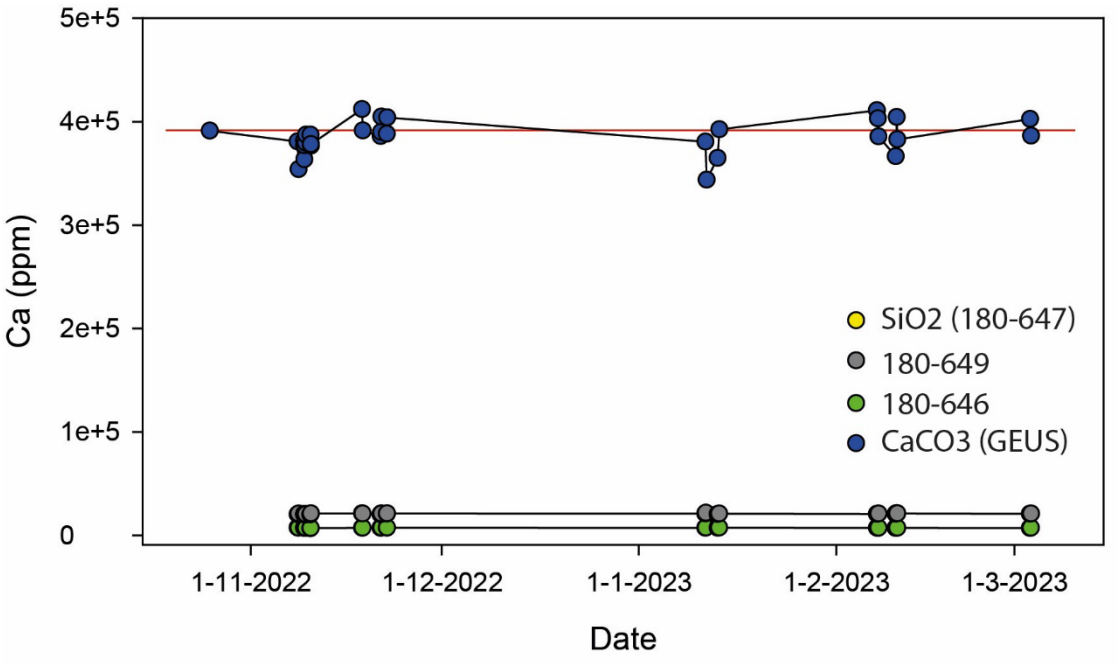

Figure 5 Analysis of Ca of four selected standards with respect to analysis time. Red line represent average.

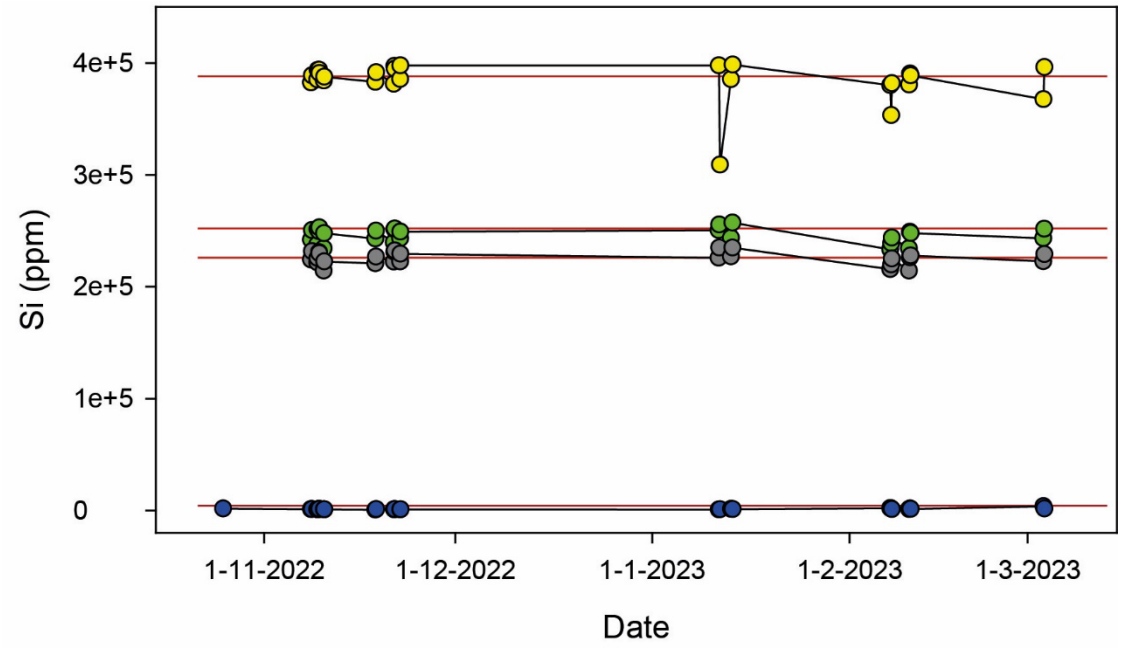

Figure 6 Analysis of Si of four selected standards with respect to analysis time. Legend as in Figure 5. Red line represent average.

However, it is important to note that the analytical reproducibility of the Nithon XL3t GOLDD+ device varies significantly across different elements in relation to their concentration in the standards, as detailed in Table 1, and that drift in analytical results is expected if more than a year differ between the analytical series.

The Nithon XL3t GOLDD+ device provides data for 43 elements, but according to Schovsbo et al. (2018), only a subset of these elements could be reliably reproduced, based on the performance with the standards. Consequently, we decided to exclude analytical results from 16 elements (Ag, Au, Bi, Cd, Cs, Hf, Hg, Mg, Pd, Re, Sb, Sc, Sn, Ta, Te, and W) that were evidently unreliable (see also Table 1).

To evaluate the reproducibility of the remaining elements, we used the ratio between the mean value and the standard deviation of the mean. For elements where this ratio was less than 5, the reproducibility was deemed too poor. These elements are typically those close to or below the detection limit. For elements with a ratio between 5 and 10, the reproducibility was considered sufficiently reliable for further analysis. For elements with a ratio above 10 the reproducibility was considered good.

Out of the remaining 27 elements, our analysis found that 16 elements (Al, As, Ba, Ca, Cr, Fe, K, Mn, Nb, Pb, Rb, Si, Sr, Ti, Zn, Zr) demonstrated good reproducibility given the targeted elemental concentrations, as judged from the standards measured. An additional 7 elements (Cu, Mo, Ni, P, S, Th, V) showed reasonable levels of measurement accuracy, while 4 elements were considered to have poor measurement quality (Cl, Co, Se, U) and were excluded for multivariate data analysis purposes (PCA).

Table 1 Analysis of reproducibility. The Mean/Std ratio was used as an indicator of reproducibility. Red indicates values below 5, suggesting poor reproducibility, Green represents values between 5 and 10, indicating acceptable reproducibility. Blue indicates values below the detection limits, particularly relevant for the pure SiO_2 and $CaCO_3$ standards. The other standards analysed are representative of soils, tills and mineralised rocks more alike the bulk composition to the cuttings that have interest here.

Element	Carbonate	180-673	180-661	180-649	180-647	180-646	PCA
	100% CaCO3				100% SiO2		
	Mean/Std	Mean/Std	Mean/Std	Mean/Std	Mean/Std	Mean/Std	
Al		31,0	21,6	20,1		19,4	yes
As		5,3	74,5	9,5		38,3	yes
Ba		28,4	34,8	41,1		16,3	yes
Ca	23,1	39,4	51,9	48,7		50,4	yes
Cl	5,5	1,7	3,9	4,3	0,3	2,6	no
Co			3,4	4,8		3,7	no
Cr		8,1	52,8	3,9		7,2	yes
Cu		23,7	6,6	8,2		23,0	yes
Fe		91,3	112,1	87,2		189,1	yes
K		99,8	78,8	77,4		95,5	yes
Mn		27,0		19,0		11,5	yes
Mo	3,9	7,7	3,6	3,9		8,4	yes
Nb		19,2	11,3	10,4		24,6	yes
Ni		6,4	5,7	9,7		4,9	yes
P		7,8	5,8	6,0		9,9	yes
Pb		24,5	60,8	7,1		15,8	yes
Rb		57,1	50,4	50,6		74,1	yes
S		12,0	6,0	7,1		8,6	yes
Se			89,1			5,4	no
Si	3,7	53,9	51,1	39,9	21,3	37,3	yes
Sr	5,9	66,4	49,9	81,0		60,9	yes
Th		5,8	5,4	8,3		30,6	yes
Ti		29,7	43,1	33,9		67,2	yes
U		4,9	3,0				no
V		9,1	12,6	6,6		5,5	yes
Zn		18,4	10,4	19,1		12,1	yes
Zr	3,2	20,4	27,3	17,2		27,6	yes

4.1 Cuttings images

Initially, photographing the samples was not part of the original project plan and was introduced on an *ad-hoc* basis early in the project. Consequently, not all samples were captured in their pre-crushed state as the crushing process had already commenced.

Initial analysis was made on selected cutting images to test if these could be used for rock type classification. The results of the tests are presented in Figures 7 and 8 and show very promising results suggesting that such analysis should be included in workflow to determine rock type variability (c.f. Figure 3) and perhaps ultimately could be used for direct seal capacity evaluation.

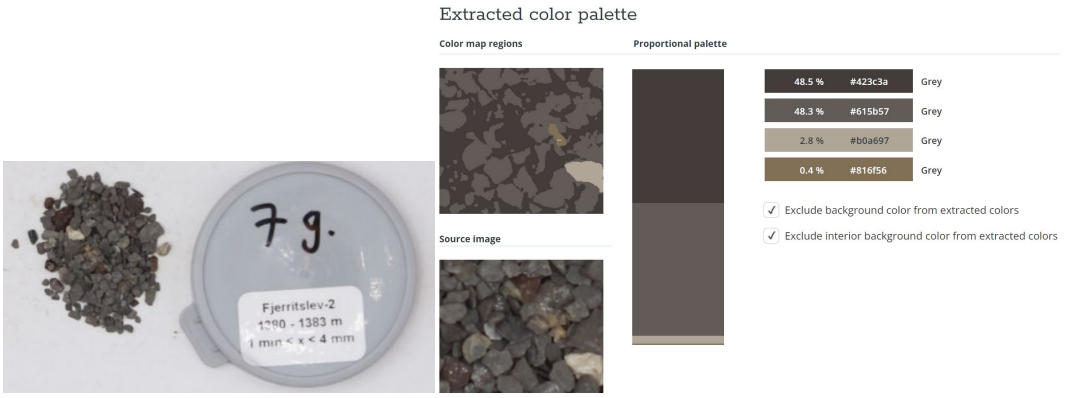

Figure 7 Example of analysis of image of the 1–4 mm cuttings fraction from 1380–1383 m in the Fjerritslev-2 well using TinEye Labs - Color Extraction Lab. The mudstone has two dominant grey colours. Less than 5 vol.% deviated from this and could potential reflect cavings or rare occurrence of rock types like concretions and/or sandy beds etc.

Figure 8 Example of analysis of image of the 1–4 mm cuttings fraction from 1280 m in the Søllested-1 well using TinEye Labs - Color Extraction Lab. The sample appears to have three dominant grey coloured shaly rock types.

4.2 Test for sample size

Testing of sample size was made on the 25th of October 2022 (measurements #326–361) using 3 powdered Paleocene mudstone samples from the Nini-4 well as test material (sample 46494, 46498, 46500 of Schovsbo et al., 2022). Each sample was measured with increasing weight and the relationship between sample size and the obtained balance, U error on the determination and content of Al, Th and K is shown in Figures 9–11. Powder was filled in an analytical cup covered with thin XRF suitable foil towards the measuring device and compressed using a handheld rod. A statistically significant non-linear regression model can be made for most of the elements and the sample weight (presented only for Al concentration and sample weight in Figure 10), but a size correction of the concentration has not been applied. Instead, it was decided to measure all samples and to omit samples with less than 2 g of material if future possible sample weight correction is possible, then the data is in house and can be corrected.

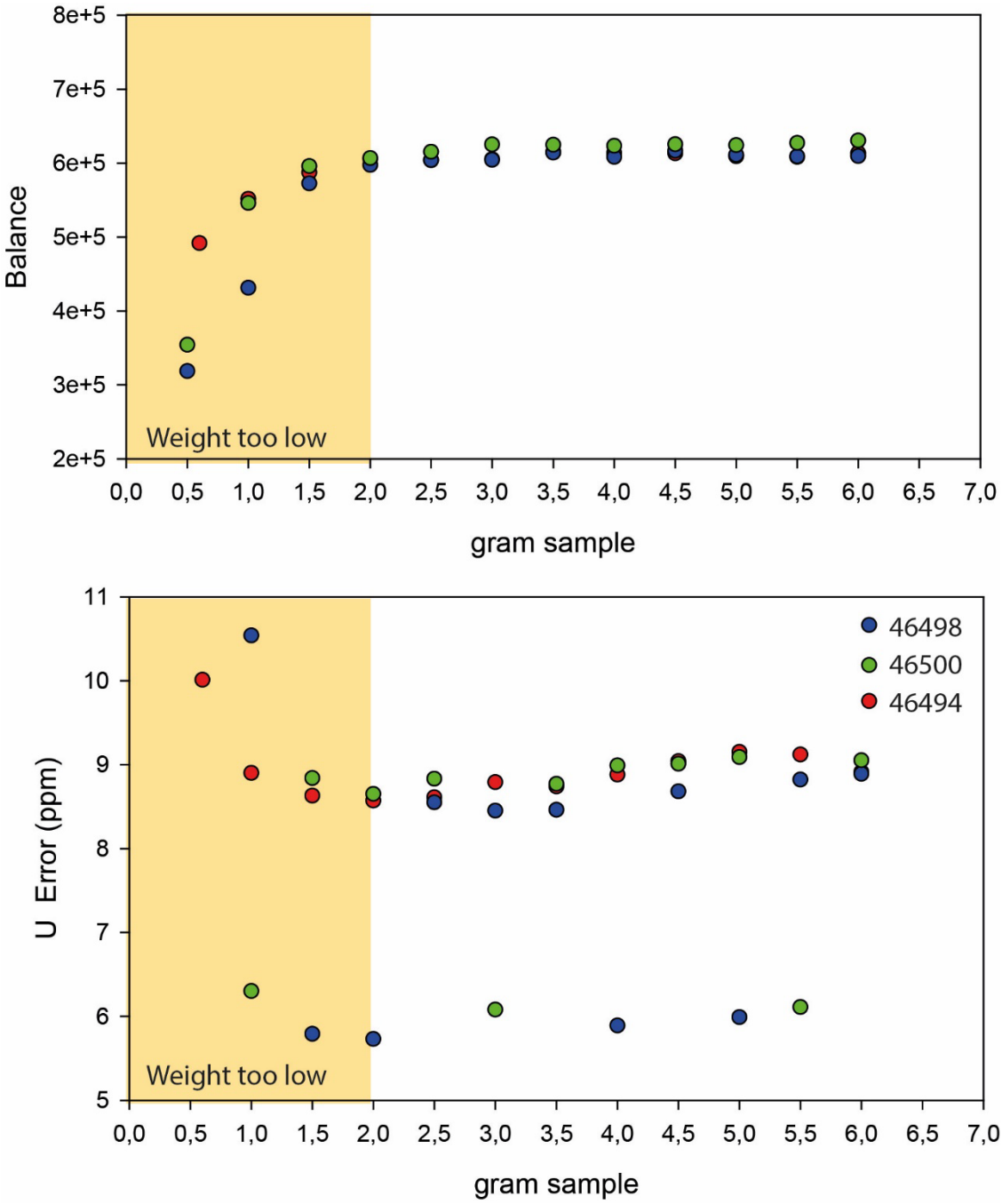

Figure 9 Balance and error on U determination dependency on sample weight. Powder was filled in analytical cup covered with special XRF suitable foil towards the Nithon XL3t GOLDD+ device and compressed using a handheld rod. Samples are from mudstone in the Nini-4 well (c.f Schovsbo et al., 2022).

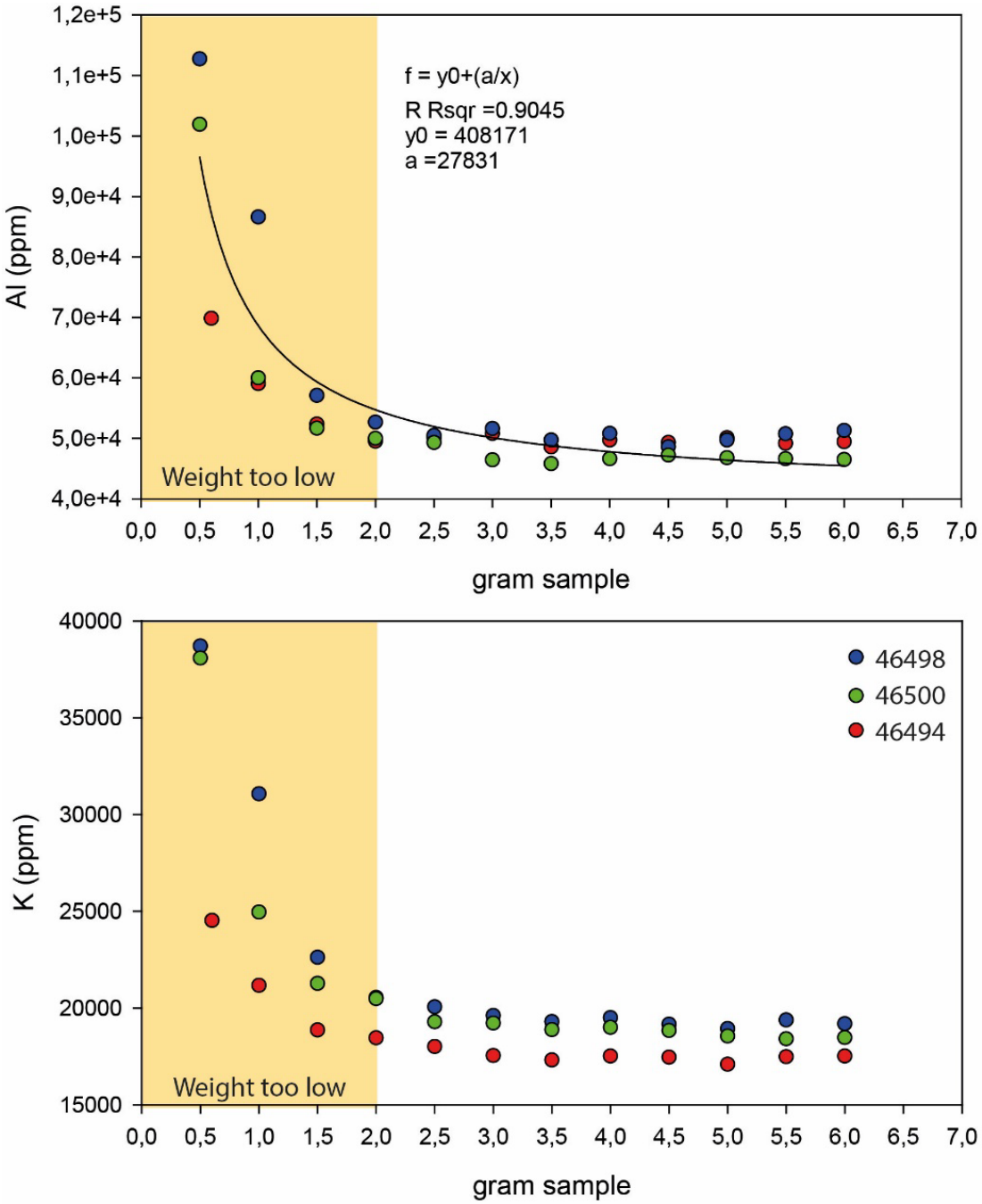

Figure 10 Al and K concentration dependency on sample weight. Samples are from the Nini-4 well (Schovsbo et al., 2022).

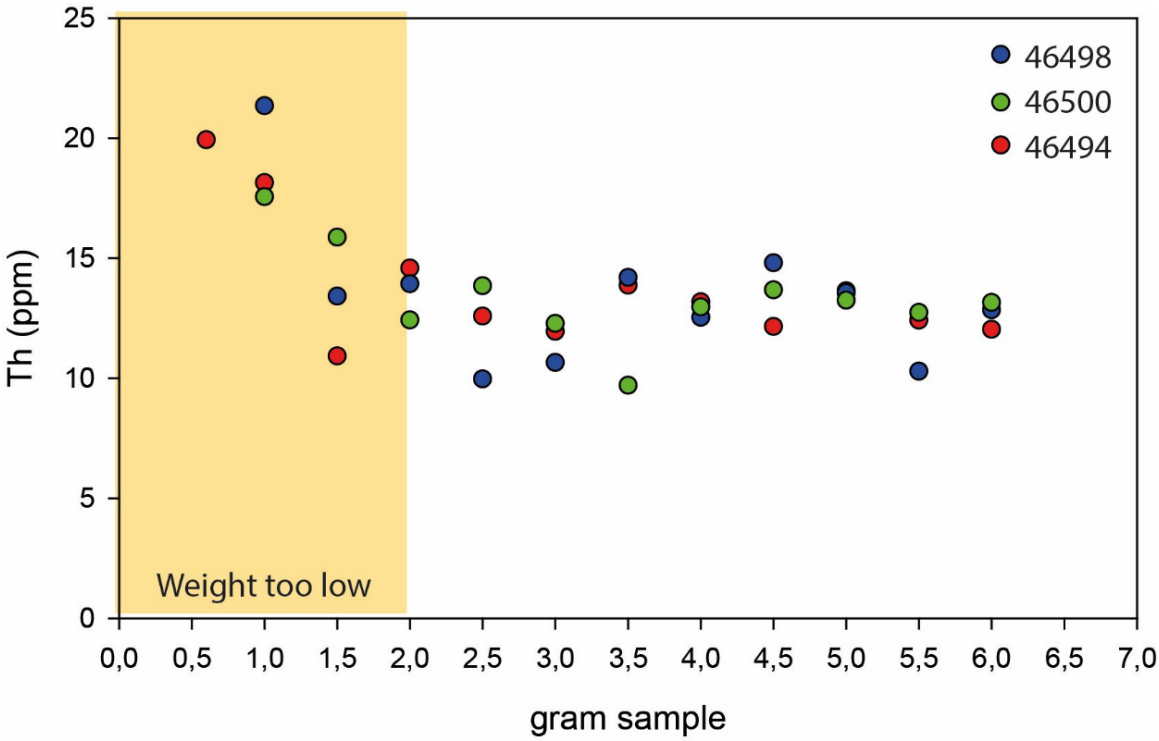

Figure 11 Th concentration dependency on sample weight. Samples are from the Nini-4 well (Schovsbo et al., 2022).

Chemical logs

Chemical log panels are presented in the following section well-by-well for selected elements to give a good impression of the key lithologies. Full data is Presented in Appendix B. The Al and Si are for example the main proxies for clay and coarser quartz (SiO_4) material (silt, sand), respectively, in the rock and the Si/Al ratio is the key ratio to examine the relative proportion between fine and coarser material. For clay mineral assemblages we use the K/Al ratio to discern between illite ($KAl_2Si_4O_{10}(OH)_2$) (high ratio) and kaolinite ($Al_2Si_2O_5(OH)_4$) or smectite group clays (ideal formular $(Ca, Mg)_{0.33}Al_2Si_{3.67}Al_{0.33}O_{10}(OH)_2$) (low ratio) dominated assemblages. Ca is the main proxy for carbonate minerals ($CaCO_3$) and S for pyrite (FeS_2) or anhydrite ($CaSO_4$).

4.3 Gassum-1 well

The well was spudded 18th of Marts 1948. Several sections in the well were cored. HH-XRF were determined from 30 cuttings samples, and 8 cuttings were imaged, in the interval 1193–1661 m, which encompasses the Fjerritslev, Gassum, and top part of the Vinding formations.

The cuttings from the Fjerritslev Formation display a high degree of colour variability, including reddish, yellow, white, and different shades of greenish grey (Figure 12). This colour variability is somewhat broader than what is typically seen in the Fjerritslev Formation and may indicate that the cuttings samples could have been mixed by cavings and/or that other processes contributed. The yellow and reddish cuttings appear to be cemented parts of the formation and a preferential loss of uncemented softer parts could have occurred.

Cuttings from the Gassum Formation contain dark greyish green and whitish grey particles likely representing mudstone and sandstone lithologies present in the formation or downfall of chalk particles.

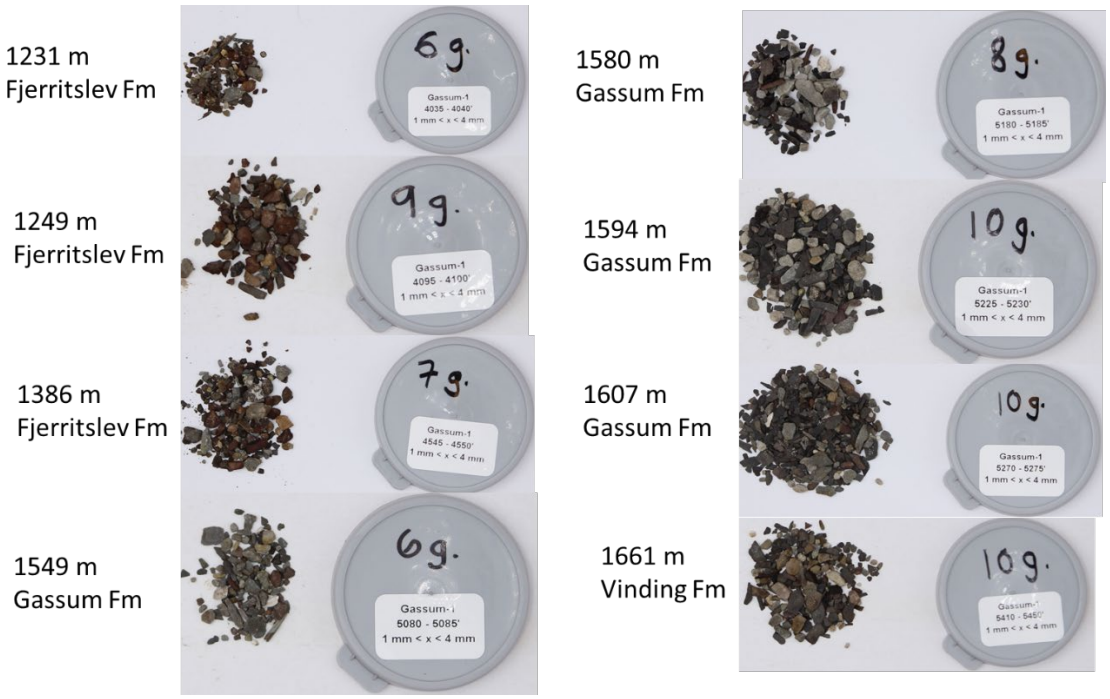

Figure 12 Selected image of the 1—4 mm cuttings fraction from the Gassum-1 well. Grey lids with marked sample size in g shown to the right have a diameter of 45 mm.

The calculated synthetic gamma-ray (SGR) from HH-XRF determinations does not tract the GR log in the well as the main parts of the Fjerritslev Formation has to low API values compared to the Gassum Formation (Figure 13). The U concentrations are generally below the level of detection which will result in a too low calculated SGR from HH-XRF determinations. The SGR_max, where the maximum API value is estimated, has much higher overall API values and track the GR motif better in the Fjerritslev Formation than the SGR for especially the lower part of the Fjerritslev and Gassum Formations (Figure 13) but fails to capture the radiogenic nature of the upper Fjerritslev Formation (Figure 13). The alignment between the GR log curve and the SGR_max below 1450 m, thus appears to be reasonably good. However, the overall impression is that the lithologies of the cuttings may be biased compared to the subsurface, being less radiogenic in the main part of the Fjerritslev and more radiogenic and clay-rich in the Gassum Formation than expected based on the GR log. In the Gassum-1 well, the GR log was the only collected well log data, thus no further information is available for comparison.

The Al and Si/Al curves more closely resemble the GR log curve, although the choice of display scales significantly influences the visual impression of the 'correlation' (Figure 13). The Si/Al ratio ranges between 2–3.5, which is also consistent with other wells penetrating the Fjerritslev Formation. The K/Al ratio in the Gassum and Fjerritslev formations is approximately 0.3 to 0.4, similar to what is measured in other sections of the Fjerritslev Formation, such as in the Vedsted-1, J-1X, and Fjerritslev-2 wells (see below), indicating that the Fjerritslev Fm in the Gassum-1 well is expected to have similar properties as observed in other wells. However, due to the generally poor quality of the cuttings from Gassum-1 well it is recommended to based future studies on the cored sections.

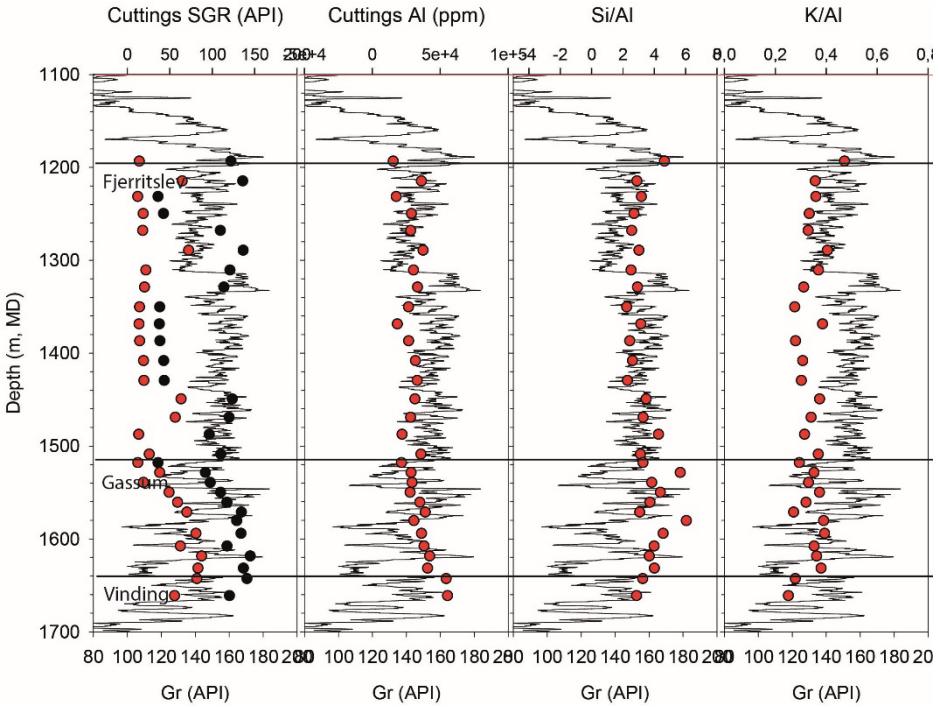

Figure 13 GR log curve and API values (red dots: SGR; black dots: SGR_max), Al content, and Si/Al and K/Al ratios derived from HH-XRF data of cuttings samples from the Gassum-1 well. It is recommended to use core material as the basis for future studies due to the poor cuttings of cuttings.

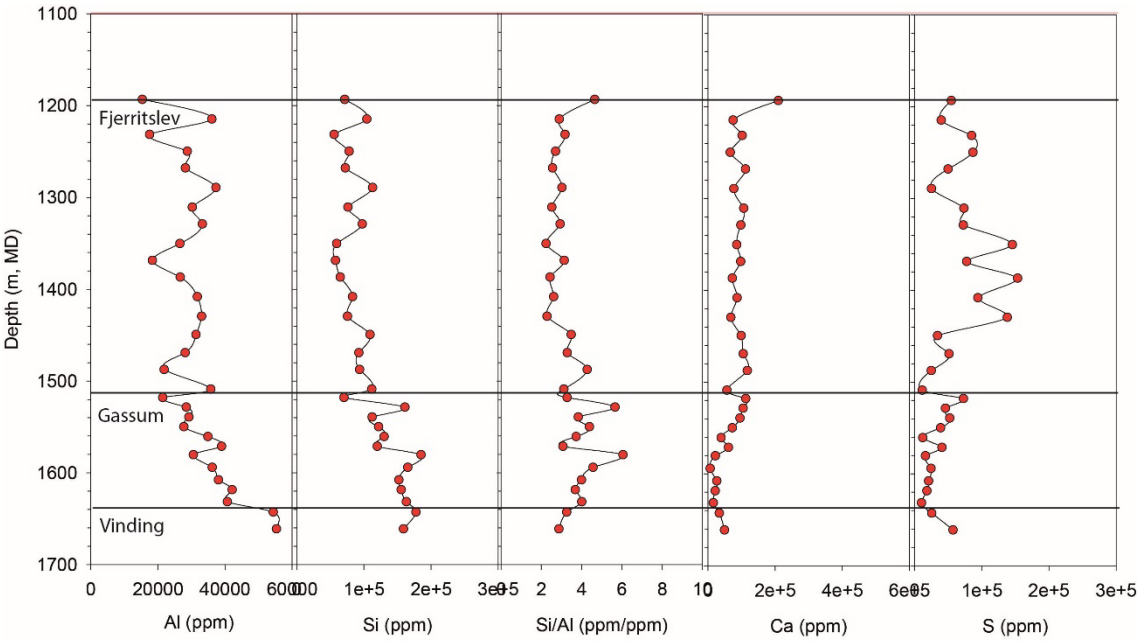

Figure 14 Elemental logs of Al, Si, the Si/Al ratio, Ca and S from the Gassum-1 well.

The TOC content through the Fjerritslev Formation is low (mean = 0.52 wt.%), and considerably higher TC values (mean = 3.97 wt.%) indicate the mudstones are fairly calcareous in agreement with the Ca log (Figures 14 and 15). Very low HI values (mean = 20 mg HC/g TOC) shows that the organic matter primarily is inertinite, corresponding to refractory carbon (Figure 15). Pyrolysable organic matter yields an average T_{max} value of 430 °C, indicating the organic matter is thermally immature.

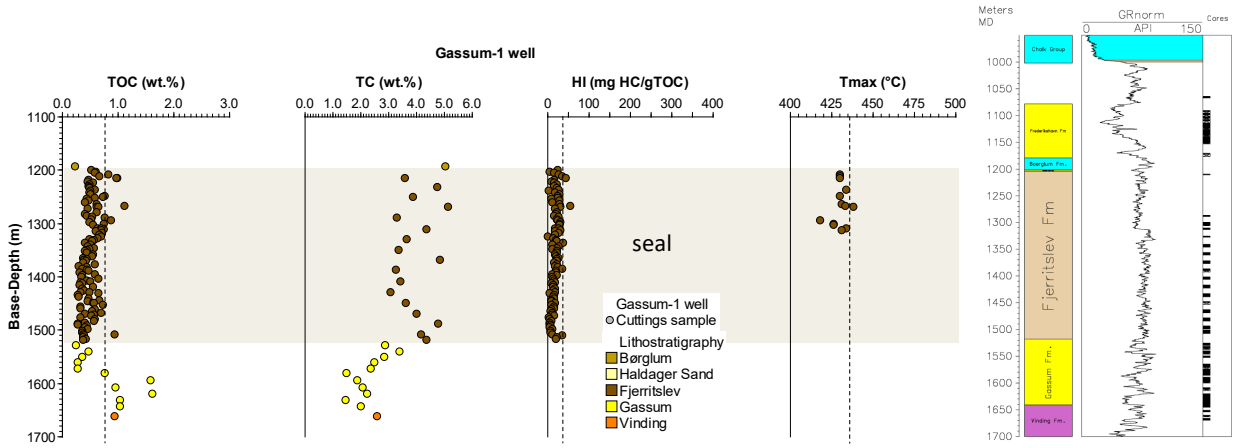

Figure 15 TOC, TC, HI, and T_{max} values in the Gassum-1 well.

Summary

The overall impression is that the cutting samples are biased compared to the subsurface apparently being less radiogenic in the main part of the Fjerritslev Formation, and more radiogenic and more clay-rich in the Gassum Formation than expected from the GR log. The GR log is the only well log measured in this well, and thus further information from other well logs cannot be

obtained for comparison. It is thus concluded that the determined cuttings chemistry is only partly representative for the subsurface strata and that analysis of the core material available both in the seal and reservoir section should be used to substantiate future seal integrity and capacity evaluations in the well.

The Fjerritslev seal is 320 m thick and is furthermore overlain by 19 m Børglum Formation mudstones. The organic matter content in the sealing mudstones is very low and thermally immature. The thick mudstone seal section with low content of dispersed, thermally immature, and inert organic matter is favourable for the seal integrity.

4.4 Fjerritslev-2 well

The well was spudded 13th of Marts 1958. Several intervals were cored in the well and HH-XRF data were collected from 96 samples (#407–502) and images was obtained from 61 cuttings (IMG_1107–1171) between 1151–2329 m, corresponding to the Gassum, Fjerritslev, Haldager and Børglum formations. Only a limited log suite (no GR log, but SP and resistivity logs) was acquired and not in the deeper part of the well (Figure 16).

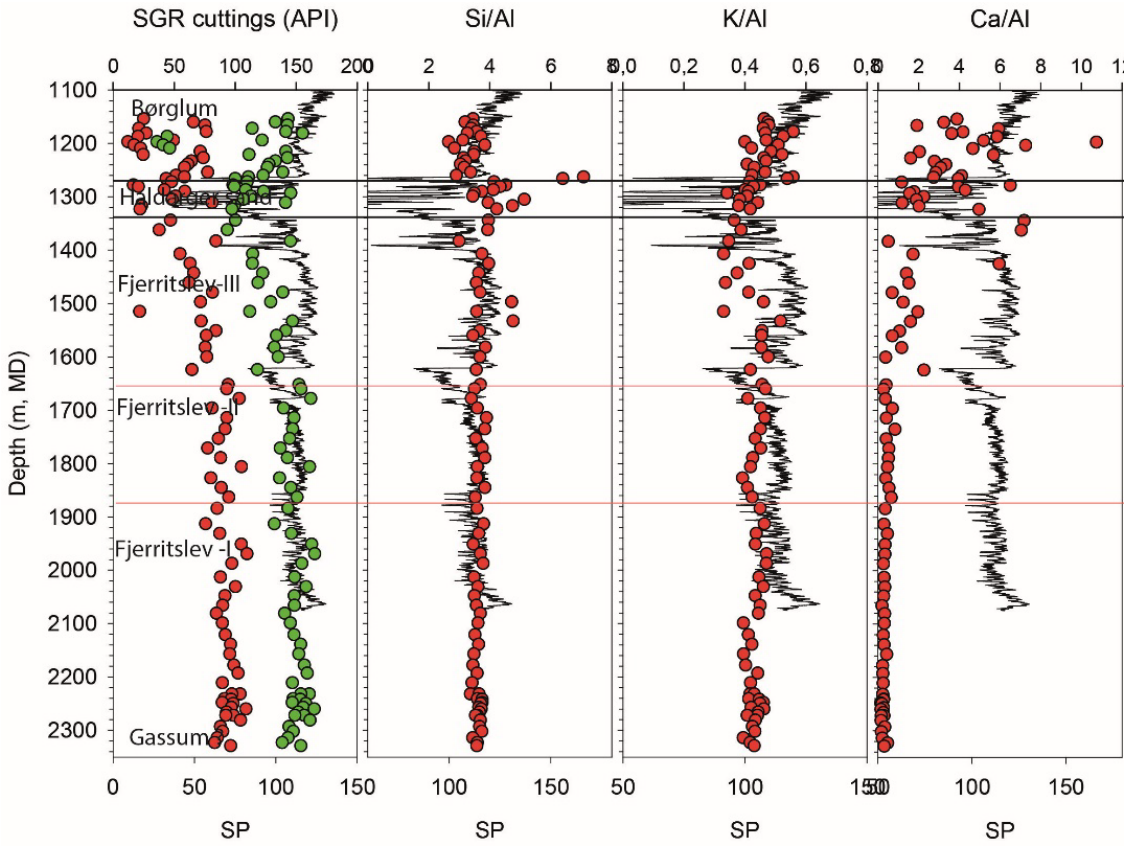

Figure 16 SP log and selected HH-XRF data in the Fjerritslev-2 well. Legend in the left panel: red dots SGR; green dots SGR_max.

An overview of the different colours of the cuttings is presented in Figure 17. Below approximately 1650 meters, the cuttings from the Fjerritslev Formation appear homogeneous and generally exhibit dark green colours, whereas above this depth, the cuttings appear more heterogeneous and with lighter colours. White-coloured cuttings, occurring in a sample from 1620 meters, are presumed to be calcareous rock fragments. In this sample the Ca/Al ration also is high (Figure 16). Given the very limited wireline rock suite acquired in the well, there is scant information to compare the observed cuttings colour variation with. The darker colours are observed in the F-I and F-II members, where also the spontaneous potential (SP) log appears to range within a narrow set of values. In the upper part of the Fjerritslev Formation (F-III and F-IV), the SP log records more variable values, which could be interpreted as a reflection of a more heterogeneous rock composition alternating between permeable and impermeable layers, known to affect the SP log response. This interpretation suggests that the colour variation observed likely

reflects the subsurface representing a the more heterogeneous nature of the Fjerritslev Formation.

Figure 17 Selected images of the 1—4 mm cuttings fraction from the Fjerritslev-2 well. Grey lids with marked sample size in g shown to the right have a diameter of 45 mm.

The U content in the Fjerrislev-2 well was generally below detection level and thus the SGR and SGR_max deviates from each other (Figure 16). The SGR and the SGR_max calculated from HH-XRF parallels each in the Fjerritslev Formation and track the shape of the SP log (Figure 16). The SGR_max appears, however, to better track the SP curve, especially in the upper Fjerritslev Formation and in the Haldager and Børglum formations. The overall fit is, however, good which supports the notion that the cuttings measured represent the *in-situ* rock.

The elemental logs in Figures 16 and 18 show in general little variation in the lower Fjerritslev Formation (below c 1700 m) and higher variation in the upper Fjerritslev Formation in agreement with the variation in colours of the cuttings and of the SP log motifs (Figures 16 and 17). The Si/Al is generally less than 4 in the Fjerritslev Formation showing a slight but steady up section increase. Highest ratios are measured in the top Haldager Formation.

The HH-XRF indicates that the greater variability of cuttings colours in the upper Fjerritslev Formation reflect more sulphide minerals (FeS_2) and carbonate (Figure 18). The Si/Al do not, however, suggest significant changes in the grain size (clay vs quartz silt/sand). In contrast to this the K/Al ratio suggests a shift towards lower ratios that should indicate a more smectitic or kaolinitic clay composition. As smectite has a much higher sealing capacity than kaolinite, this will be

relevant to analyse further. The data from the Vedsted-1 well showed likewise an increase in smectite content in the upper part of the Fjerritslev Formation (Mbia et al., 2014).

The Gassum Formation does not from the HH-XRF data appear to be quartz rich. In the well the only quartz rich unit appears to be the top Haldager Formation (Figure 16 and 18). A core in the base of the well cut in the Gassum Formation show, however, that sand is present here. The lack of a respond in the HH-XRF for sand in the Gassum Formation could be because only the 1—4 mm size fraction is investigated and not the finer fractions where fine grained sand particles will potential fall if the sandstone is not strongly consolidated or cemented. Hence in future studies care should be given to examine all size fractions.

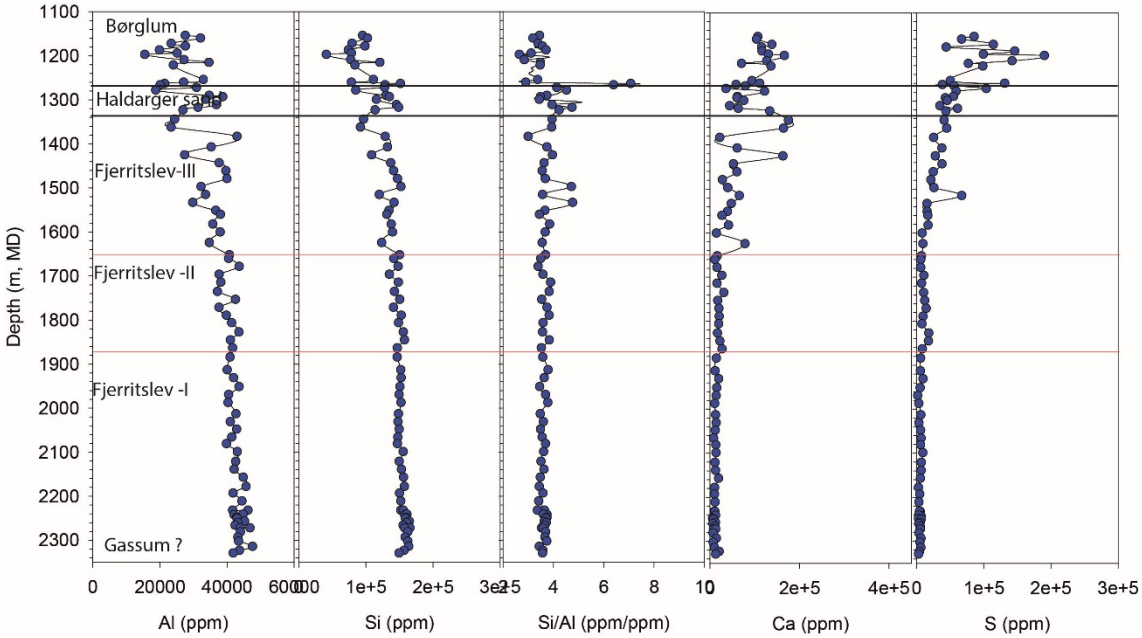

Figure 18 Elemental logs of Al, Si, the Si/Al ratio, Ca and S from the Fjerritslev-2 well. Note that the lack of high Si in Gassum could be due to fractionation of lithologies with cutting size fractions. Here only the 1—4 mm size fraction is investigated and thus the data is likely biased towards cemented lithologies thereby supressing unconsolidated sand and soft clay.

The HI values are generally <125 mg HC/g TOC and has a mean of only 85 mg HC/g TOC (Figure 19). However, HI shows an increasing trend from the base of the F-I Member to a maximum of 205 mg HC/g TOC in the F-III Member from where it decreases again towards the top of the Fjerritslev Formation (Figure 19). The TOC content is overall low (mean = 1.02 wt%) with the highest contents measured in the F-III and F-IV members. This is aligned with the generally higher organic matter preservation potential in the upper part of the Fjerritslev Formation (Petersen et al., 2008), indicating more reducing and oxygen-deficient depositional conditions and in agreement with the higher content of S (probably pyrite) recorded by the HH-XRF data (Figure 18). The likewise higher carbonate content is underpinned by the considerably higher TC content compared to TOC (Figure 19). T_{max} values average 428 °C indicating the organic matter is thermally immature.

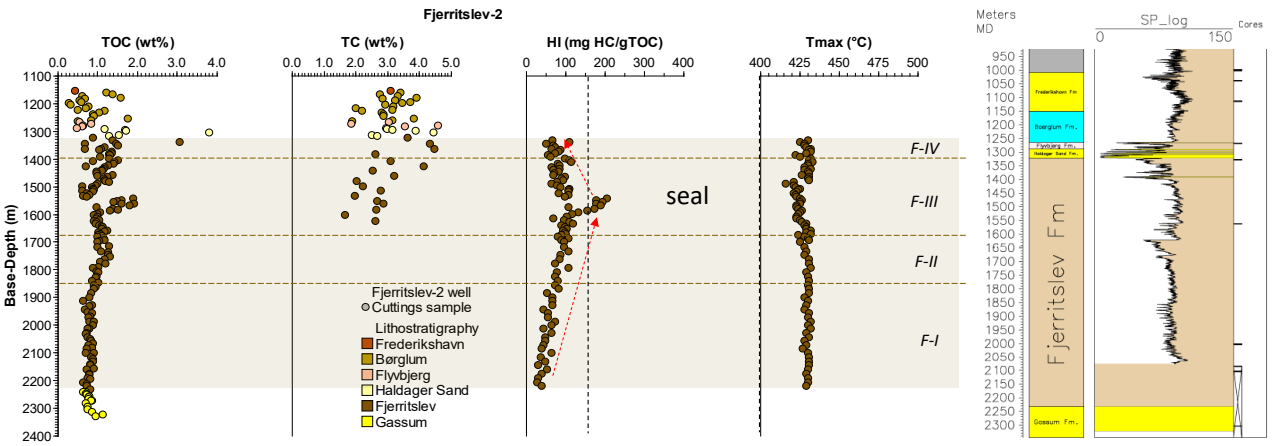

Figure 19 TOC, TC, HI, and T_{max} values from the Fjerritslev-2 well.

Summary

The clay-rich 911 m thick mudstones of the Fjerritslev Formation constitute a substantial seal which is reinforced by the possibly more smectitic clay composition in the upper part. The low content of dispersed, refractive and thermally immature organic matter is favourable for the seal integrity due to a low risk for the organic matter to form a coherent organic network in the rock matrix that could lower the seal capacity towards supercritical (sc)CO_2.

4.5 J-1X well

The J-1X well was spudded 24th of December 1969. No cores were cut. 64 HH-XRF determinations were measured, and 55 cuttings images were recorded (IMG_1044–IMG_1098) between 1100–2000 m encompassing the Fjerritslev, Gassum and Vinding formations.

Images of the 1–4 mm cutting fraction are shown in Figure 20. All cuttings samples show a mixed assemblage of shapes and sizes. Many cuttings are elongated and to the authors best opinion do not resemble rock chips from the well bore but instead resemble cavings.

The Gassum Formation (cutting depth 1734 and 1780 m in Figure 20) is characterised by mixed mudstones and sandstone types reflecting that sand and mudstone beds intercalate in the formation. The cuttings represent 10 m intervals which is on par with the thickness of the sandy beds, and it can thus not be expected that the cuttings sampling interval will "clean-up" and capture such relatively rapidly changing lithologies fully. Cuttings from the base of and below the Gassum Formation (1969 m) and Vinding Formation (1978 m) are characterised by the occurrence of red mudstone fragments with or without quartz sand. Cuttings from the Fjerritslev Formation are characterised by dark grey-green rock chips that in part consist of quartz grains (cf. 1612 m). In the top part red mudstone fragments appear (c. 1316 m).

Figure 20 Selected images of the 1–4 mm cuttings fraction from the J-1X well. Grey lids with marked sample size in g shown to the right have a diameter of 45 mm.

SGR and Gamma ray log

A wireline log panel is shown in Figure 21 for the J-1X well.

The caliper log shows that there are numerous zones with borehole enlargement along the J-1X borehole. With respect to the size and shapes of the cuttings described above, there is no doubt that material from these enlarged borehole sections is now present in the cuttings samples as cavings.

Comparison of the cuttings SGR and GR show a quite variable relationship (Figure 21). In the mid part of the Fjerritslev Formation the fit is quite good, in the basal part and in the Gassum Formation it is reasonable, and in the upper part of the Fjerritslev Formation it is poor. The SGR and GR variation also agrees well within the mid part of the Fjerritslev Formation where an enlarged borehole sections occur.

The misfit between SGR and the GR log in the upper part of the Fjerritslev Formation correspond to the interval where the formation is enriched in more labile organic matter as reflected by TOC and relatively higher HI (see discussion of these data). We thus suspect that U here will contribute more to the GR signal. As mentioned previously U is, however, poorly measured by the HH-XRF instrument. One could thus suspect that the poor fit between SGR and GR reflects a shift in the proportion of U to the total radioactive signal (NORM) i.e. from dominantly from K and Th and to dominantly from U. This could be ascribed to more K poor clay such as kaolinite and smectite and/or a higher U content as mentioned above or both. This assumption should be validated by measuring the samples by ICP-MS/OES for high quality determinations of U, K and Th and by measuring the mineralogical content.

In the Gassum Formation there is a reasonable god fit between SGR and the GR log in the Gassum Formation. The Gassum Formation consist of alternating sandy and muddy intervals. The colour of the cuttings all show mixed lithologies from the Gassum Formation similar as the chemical logs show mix sand-mud signal, however with a tendency towards the clay-rich component. This lithology likely has a higher chance of ending up in the 1—4 mm size fraction than unconsolidated silt- and sandstones. Hence, it is suggested to analyse all cuttings size fractions for a better understanding of the distribution and properties of the Gassum Formation including grainsize, sorting and degree of cementation.

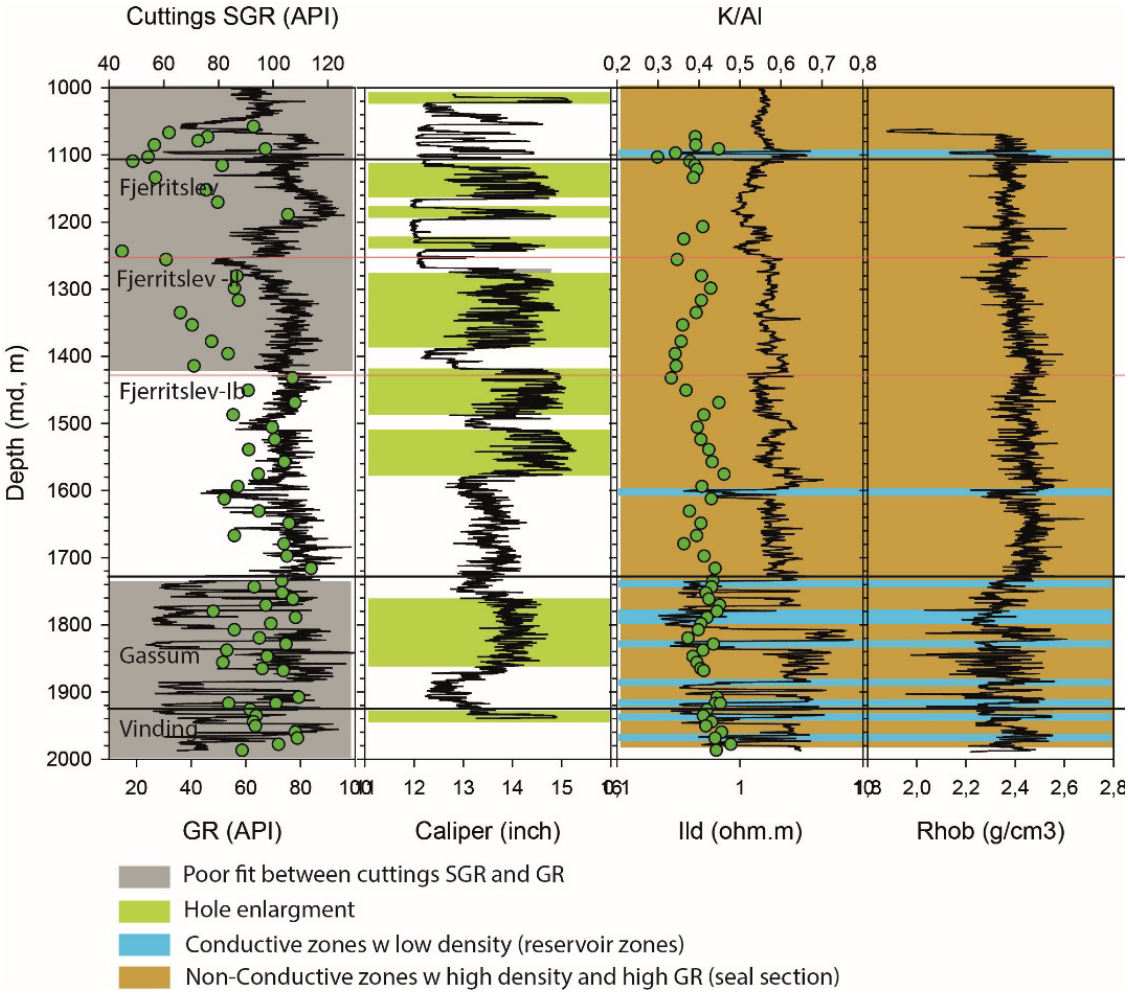

Figure 21 J-1X wireline logs and cuttings SGR calculated from HH-XRF determination of U, Th and K. Correlation between SGR and GR is shown. It is recommended to conduct more precise determinations of U, K and Th to better evaluate the cuttings API value and to conduct measurements of cuttings fractions separated into sand and mudstone to examine the range in API for better interpretation of mixed lithologies, such as in the Gassum Formation.

The Al content in the J-1X well peaks in the mid part of the Gassum Formation and in the lower and mid part of the Fjerritslev Formation (Fig. 22). From 1400 m the Al content decreases stratigraphically upwards. The Si content shows two distinct peaks: one in upper Gassum Formation and one in the Fjerritslev Formation around 1500 m. The Si/Al ratio shows high values in the Gassum Formation in samples that visually also contain mixed sand/mudstone lithologies (cf. Figure 20). In the Fjerritslev Formation, the Si/Al ratio is upward stable or weakly decreasing until 1500 m before the ratio stabilise at low values from 1450 m and upwards. The raised Si/Al values coincide with samples which contain quartz grains and the Si/Al ratio is interpreted to reflect relative increases in coarser quartz rich material in an otherwise clay dominated matrix.

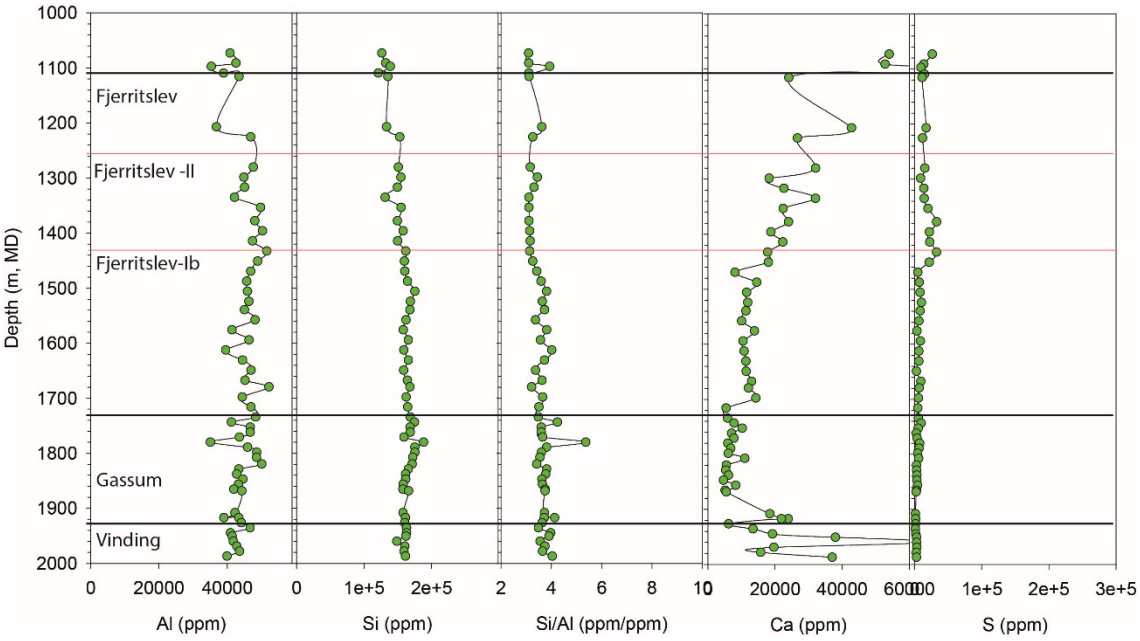

Figure 22 Elemental logs of Al, Si, the Si/Al ratio, Ca and S from the J-1X well. As a proxy for the non-siliciclastic component Ca and S are shown, but Fe, Mn and Mg would also be of relevance.

The Ca content show a trend that are remarkedly close to outline the top and base of the Gassum Formation (Figure 22) since both the Vinding (and lowermost Gassum) and base Fjerritslev Formation have higher Ca values than those measured in the Gassum Formation. In the upper Fjerritslev Formation (from 1500 m) the Ca show a remarkable steady increasing upwards trend with peak values in the Haldager Formation.

The cuttings with elevated Ca content also contain reddish coloured rock chips and it is suspected that the enrichment in Ca stems from these parts. This could be validated from thin section and/or from simple experiments with treatment of the rock chips with cold and hot acid to examine if carbonate is present and if it is calcite, siderite and/or ankerite.
S shows a marked enrichment in the mid to upper Fjerritslev Formation where the level range typical between 1-2.5 wt.%. This rise is within the interval of the Fjerritslev Formation where also TOC and HI increases (Figure 23) and may signal enhanced active sulphate reduction due to oxygen-deficiency caused by higher productivity and nutrient availability, and/or preservation potential of organic matter. The TOC content is overall low (mean = 1.04 wt%), but the highest values are measured in the topmost F-II Member and the F-III Member (Figure 23). This increase is accompanied by an increasing HI trend from the lower F-II Member to a maximum of 303 mg HC/g TOC in the F- III Member. These are original values since the organic matter is thermally immature (mean T_{max} = 431 °C).

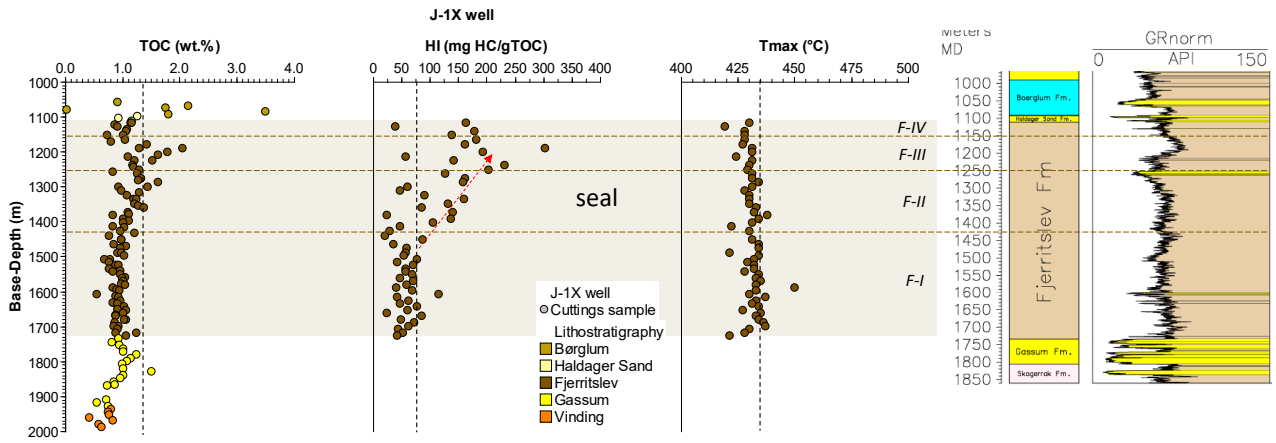

Figure 23 TOC, HI and T_{max} from the J-1X well.

Summary

The Fjerritslev Formation constitutes a 623 m thick seal divided by the first porous beds from 1600–1610 m into a c. 120 m thick primary seal and a c. 500 m tick secondary seal. Additional porous beds exist in the secondary seal c.f. gamma ray low at 1250 m. The TOC content is overall low and is composed of immature dispersed organic matter, which is favourable for seal integrity.

Reservoir units exist at all stratigraphical levels, i.e., in the Vinding, Gassum and Fjerritslev Formations in the J-1X well. These reservoir units can be identified on wireline logs and from cutting pictures as containing quartz grains and by having low formation resistivity, low formation density, and a low natural radioactivity as seen by low GR log readings. Cuttings from these intervals contain sand sized quartz particles.

Mudstone sections in J-1X that will act as seal can be identified in all investigated formations. These sections are characterised by wireline logs having high formation resistivity, high formation density, and high natural radioactivity reflected in high GR log readings. Cuttings from these intervals are all dominated by mudstone lithologies with variable carbonate content. Within the mudstone part of the Fjerritslev Formation two main rock types exists. In the lower part (1734– c. 1450 m) a clay dominated low carbonate rock type exist. This type grades into an upper type characterised by presumably higher clay content and higher Ca, S and TOC contents (Figure 22 and 23).

In terms of seal units in relation to a CO_2 storage in the Gassum Formation, the first porous beds in the interval 1600-1610 m in the Fjerritslev Formation in the J-1X well provides the natural separation between the primary Fjerritslev Formation seal (c. 120 m thick in J-1X) and the secondary seal composed of the remaining mudstones of the Fjerritslev Formation (c. 500 m thick in the J-1X). From the petrophysical interpretation, however, this section appears to contain impure sandstones from c 1252–1262 m.

4.6 Vedsted-1 well

The Vedsted-1 well was spudded 9th of May 1958, several intervals were cored but only the SP log was measured in the well. A total of 72 HH-XRF determinations and 73 cutting images were recorded (IMG_0971–IMG_1043) between 1025–2062 m encompassing the Flyvbjerg, Haldager, Fjerritslev, Gassum, and Vinding formations.

In the Vinding, Gassum, and Fjerritslev formations, the cuttings in the 1–4 mm fraction are predominantly dark green to grey, with the occasional presence of dark reddish grains (Figure 24). In the Gassum Formation, the cuttings exhibit lighter green colours with more, but still subordinate, grains of light, apparently siliceous nature. A cutting sample from 1800 m in the Fjerritslev Formation appears to contain a very mixed assembly of coarse grains consisting of green, red, and light-coloured grains, many of which seem cemented (Figure 25).

Figure 24 Selected images of the 1—4 mm cuttings fraction from the Vedsted-1 well. Grey lids with marked sample size in g shown to the right have a diameter of 45 mm. Note that the depth unit is meter but is mistakenly marked as feet (‘).

Figure 25 Cuttings from 1800 m (IMG_0992) in the Fjerritslev Formation, Vedsted-1 well. The sample has the highest Si/Al ratio in the Fjerritslev Formation and represents an interval with SP log readings that are markedly different the rest of the mudstone section. Grey lid shown to the right have a diameter of 45 mm. Note depth in meter (incorrectly shown as feet).

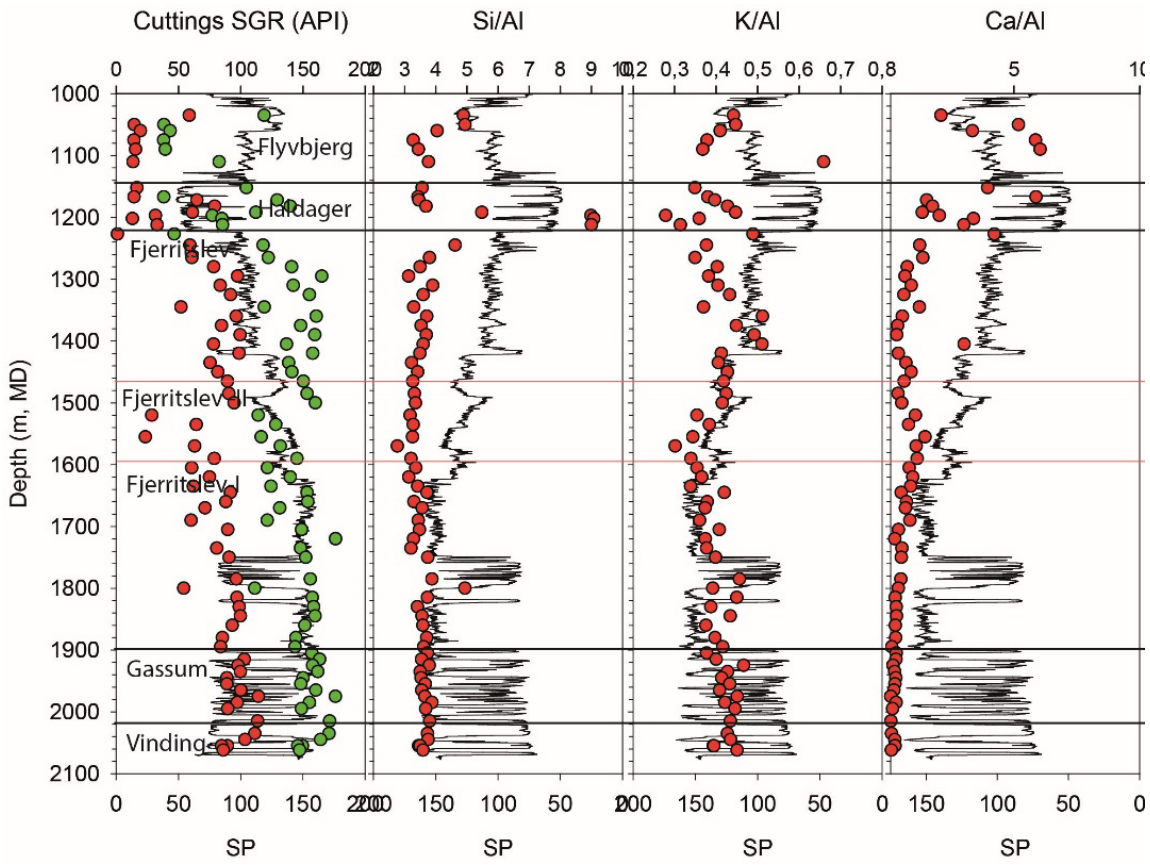

Figure 26 Logs and HH-XRF data from the Vedsted-1 well. Note that the SP curve is plotted with revers scale in the 3 panels from right.

The U content in the Vedsted-1 cuttings samples is below level of detection and the cuttings SGR and SGR_max logs thus do not coincide but track each other (Figure 26). The SGR log mimic the

log motif from the SP log particularly well from the Fjerritslev II member and below. In the upper part of the well, in the Flyvbjerg Formation and upper Fjerritslev, the misfit between the curves is larger. In the Flyvbjerg Formation, the SGR is lower than in the Fjerritslev Formation whereas the SP log show similar values as in the Fjerritslev Fm. The SGR_max in the Flyvbjerg Formation range up to similar values as in the Fjerritslev Formation suggesting that misfit is due to poor U determinations or selective loss of uranium rich clays as discussed for other wells.

In Figure 26, other element data are compared to the SP curve. The SP curve is sensitive to permeability changes. High Si/Al ratio coincide with SP shift in the Haldager Sand Formation and Fjerritslev I Member suggesting that these beds are permeable due to the presence of coarser quartz material. We do not however see a relationship in the Gassum Formation between Si/Al and the rapid alternating values of the SP curve that suggest thin permeable beds occur interbedded with impermeable beds. Such lack of sensitivity in the Si/Al ratio was also observed in the Fjerrislev-2 well where it was suggested that the 1–4 mm size fraction do not adequately sample sand grains and that a full evaluation of the whole cuttings sample should be made.

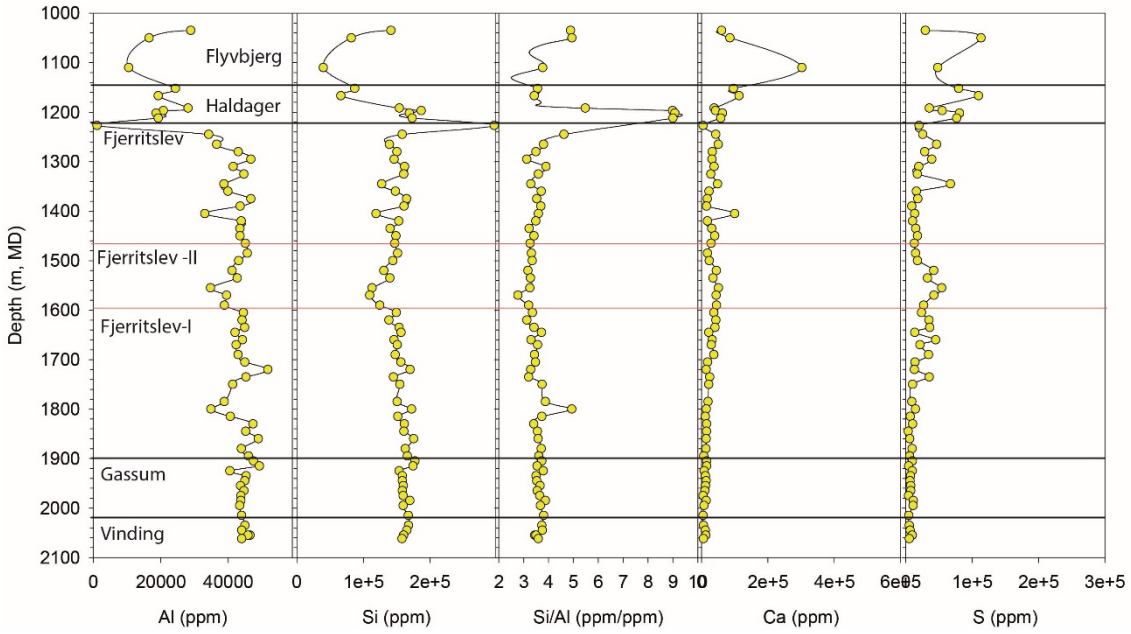

Figure 27 Elemental logs of Al, Si, Ca and S contents (ppm), and the Si/Al ratio in the Vedsted-1 well.

Apart for permeability the SP log is also sensitive to bulk cation exchange capacity (CEC) of the rock as the SP signal are proportional to the CEC contract between layers. CEC correlates to the specific surface area which is particularly high in clay minerals as this group have the largest internal and external surfaces. Lowest CEC characterise kaolinite and highest values smectites. In Figure 26 the K/Al ratio of the SP curve are compared. In the top part of the well and down to c. 1350 m the relationship between SP and K/Al appear poor and revers compared to the relationship below 1350 m where the relationship appears to be very good. In this part of the well the K/Al ratio mimic each other very good. Low K/Al ratios in the Fjerritslev thus also represent high SP values (note SP scale shift in Figure 26) that could reflect shift in clay assemblage to more smectitic having high CEC and low K/Al ratio.

If this interpretation is correct, then it is an outstanding issue to explain the relationship between K/Al and SP in the upper part of the well. One part of the explanation could be hinted at by the Ca/Al log shown in Figure 26. According to this log the Flyvbjerg and Haldager formations are carbonaceous which apparently this influences the SP to show lower values that otherwise expected from the SGR and K/Al ratio logs. The upper part of the Fjerritslev Formation is, however, not particularly carbonaceous. This part has slightly higher S content (Figure 27) but has somewhat variable and low TOC content that has a very low HI index suggesting a shift in depositional environment and perhaps type of organic matter that is atypical for the upper most Fjerritslev Formation as seen elsewhere (c.f. compare Figure 23 and 28).

The TOC content is generally low with a mean of 0.86 wt% and the values reached in the topmost F-II and basal F-III members (Figure 29). The HI is for most samples <100 mg HC/g TOC, again maximising in the topmost F-II and basal F-III members. A mean T_{max} value of 429 °C shows that the organic matter is thermally immature.

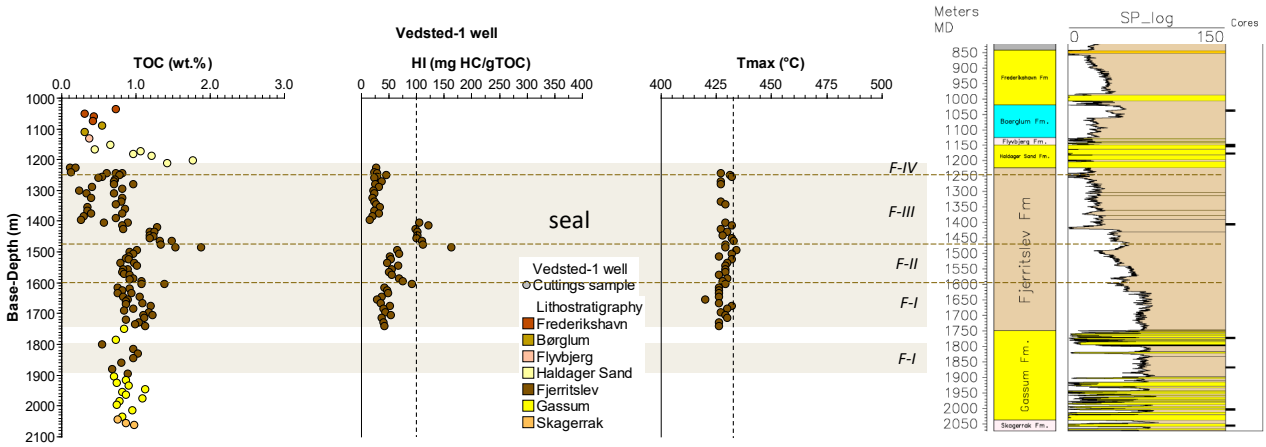

Figure 28 TOC, HI, and T_{max} values of the Vedsted-1 well.

Summary

The Fjerritslev Formation is 674 m thick mudstone section with a low TOC content composed of immature dispersed largely non-reactive organic matter, which is favourable for seal integrity. Permeable coarse beds exist in the lower part of the formation (c.1750-1800 m) that may act as a natural compartmentalisation of the Fjerritslev Formation complex in a lower primary seal and upper seal section that range up to the permeable beds of the Haldager Formation. The seal sections likely contain smectite clays that have a high seal capacity due to its high surface areas and small particle size.

4.7 Vinding-1 well

The Vinding-1 was spudded 17th of July 1947. Material was insufficient for HH-XRF determination. 16 cuttings images (IMG0737–IMG0763) were recorded between 1469–1648 m (4820'–5410') encompassing the Fjerritslev and Gassum formations.

Cuttings from Vinding-1 well were all low in weight and thus it was decided not to analyse them for HH-XRF. The cuttings from Fjerritslev formation are all multi-coloured showing reddish and greenish colours (Figure 29). Cuttings from Gassum Formation contain lighter coloured grains that appear to be cemented sandstone.

Figure 29 Selected images of the 1—4 mm cuttings fraction from the Vinding-1 well. Grey lids with marked sample size in g shown to the right have a diameter of 45 mm.

Only the F-I Member of the Fjerritslev Formation is preserved, and the member has a very low TOC content with a mean of only 0.57 wt% (Figure 30). The HI values are likewise very low with

a maximum of 35 mg HC/g TOC, testifying to refractory kerogen. Few T_{max} values show the organic matter is thermally immature.

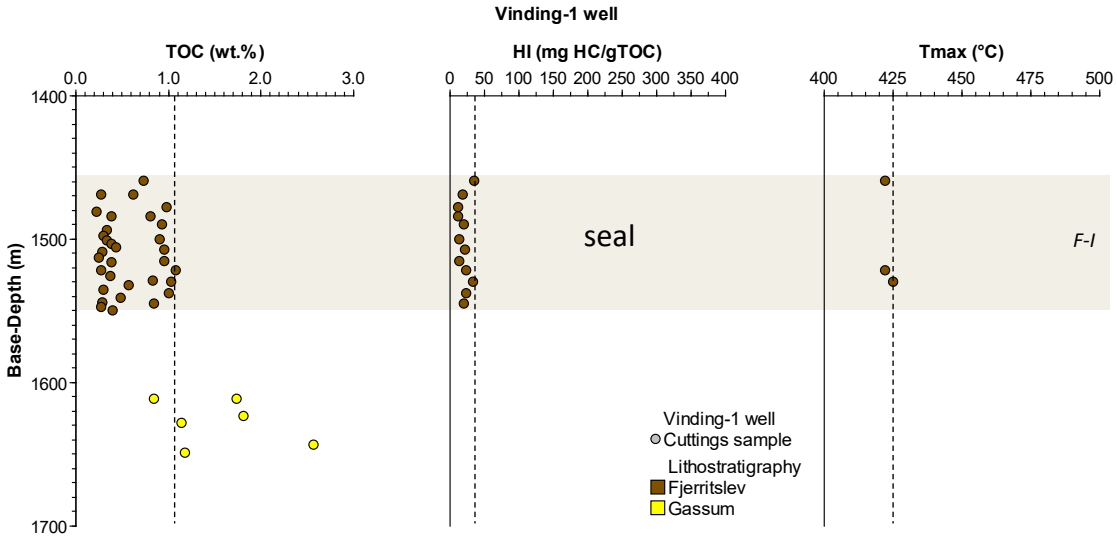

Figure 30 TOC, HI, and T_{max} values of the Vinding-1 well.

Summary

The Fjerritslev F-I Member seal in the Vinding-1 well has a substantial thickness of 142 m plus an addition of 86 m of an undifferentiated Jurassic section. The thick mudstone section contains dispersed, thermally immature, and inert organic matter which is favourable for seal integrity.

4.8 Rødby-1 well

The Rødby-1 well was spudded 1st of November 1958. Many cores were cut, but only a limited wireline log suite including the GR and caliper logs was acquired. The hole condition is generally good and no large fall-out zones were identified as the hole diameter varies between 8–10 inch for the studied section. A total of 76 cuttings were analysis (sample 934–1045) and 95 cuttings images (IMG_0877–IMG_0970) were taken between 760–1380 m representing the Falster, Ørslev, Bunter Sandstone and top Bunter Shale formations.

The lithologies in the cutting samples are generally light grey to reddish coloured mudstones (Figure 31) and are thus markedly different from those present in the Jurassic section, i.e., the Fjerritslev Formation (c.f. Figures 7, 17). The Falster Formation and the top Ørslev Formation are generally very light grey (950 m and 998 m, Figure 31) consistent with a lithology dominated by carbonate and anhydrite as suggested by HH-XRF data (Figure 32). Cuttings from the interval with high GR API readings and Al levels Ørslev Formation (c.f. 1065 m and 1095 m, Figure 33) are darker coloured in agreement with the presence of more clay-rich material in the cuttings.

Cuttings from the Bunter Sandstone Formation range in colours from light grey to reddish (e.g., 1196 m, 1232 m, and 1260 m; Figure 31). Millimetre sized sand grains were seen in the sample from 1232 m (Figure 33), consistent with a very quartz rich composition as judged from the HH-XRF measurements.

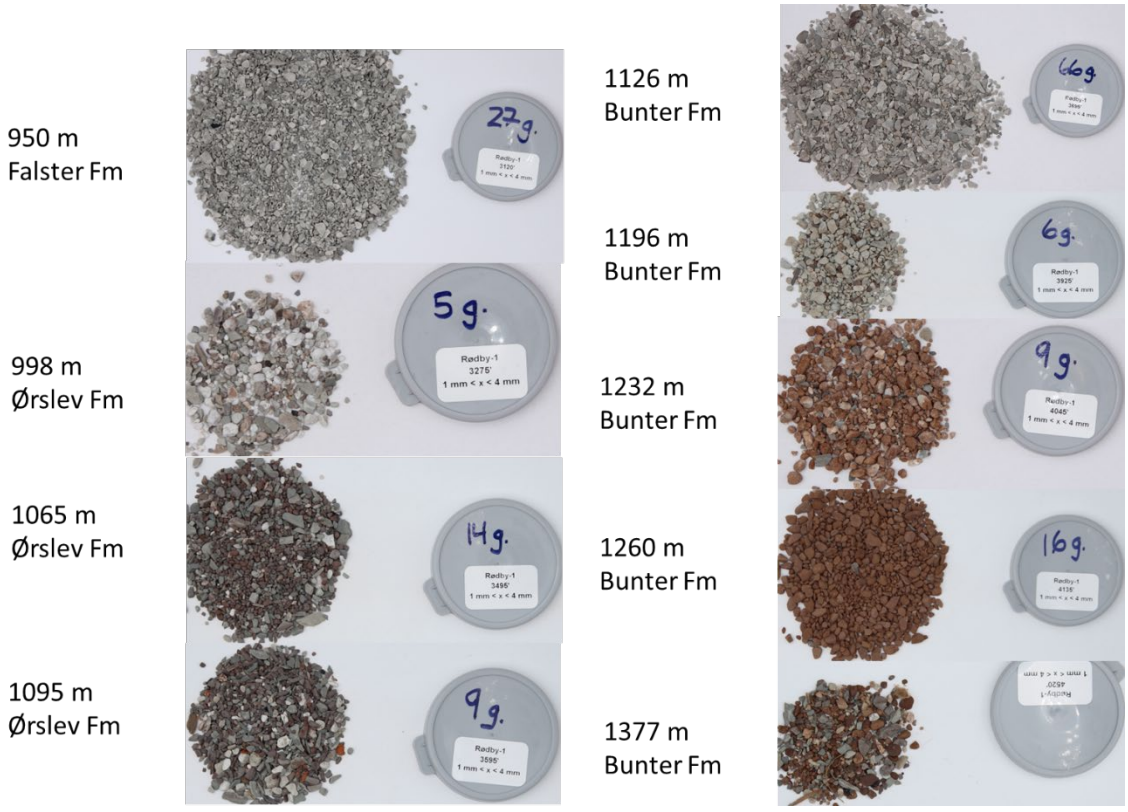

Figure 31 Selected images of the 1—4 mm cuttings fraction from the Rødby-1 well. Grey lids with marked sample size in g shown to the right have a diameter of 45 mm.

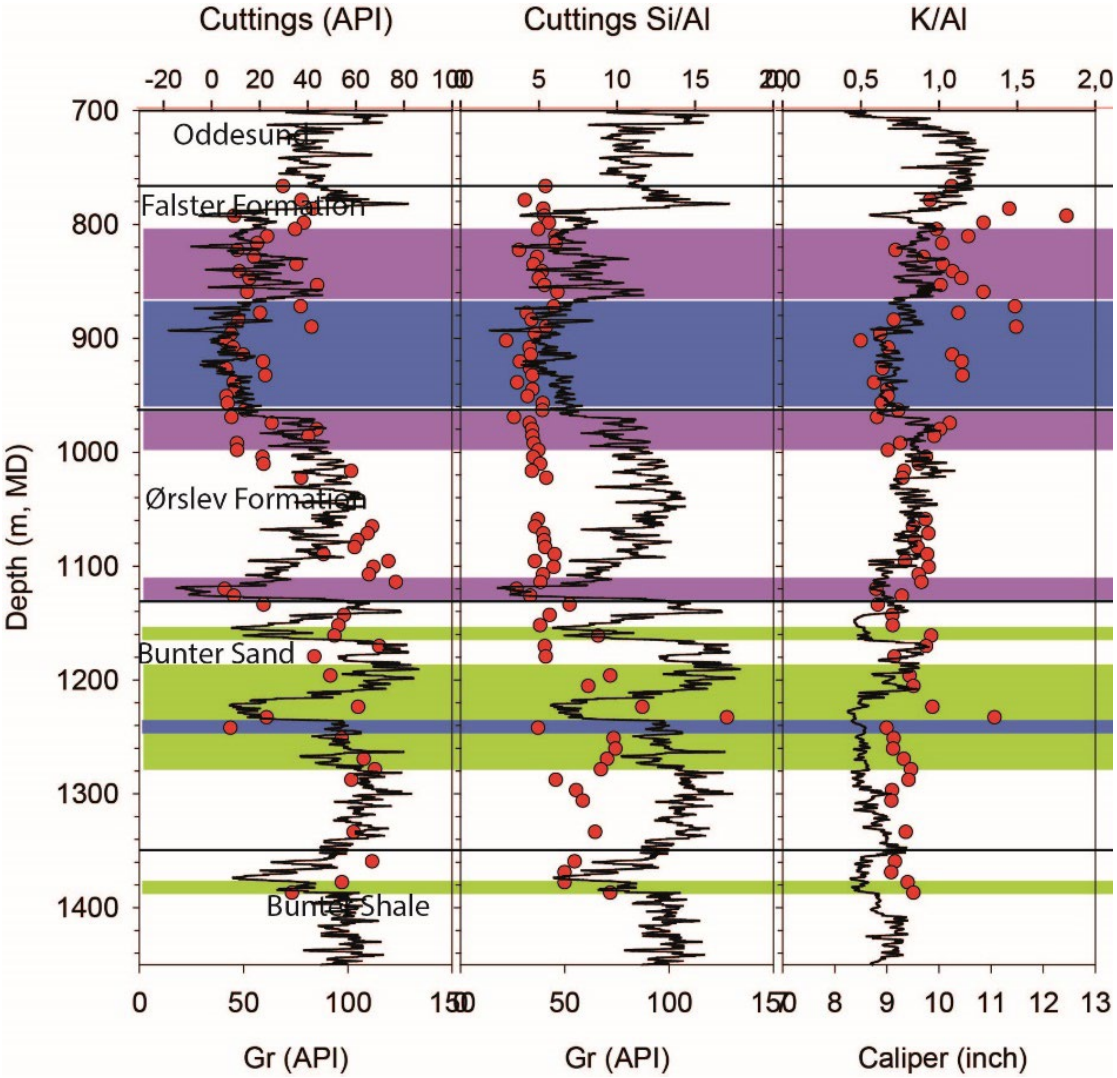

Figure 32 GR log curve, caliper log and API values calculated from cutting samples based on HH-XRF data (SGR; SGR_max not shown) in the Rødby-1 well. The visual fit between SGR and GR API is in most intervals good. Lithologies are anhydrite (purple), carbonate (blue) and sandy (yellow). Red dot: cuttings measurement. K/Al ratios >1 in Bunter Sand Formation and the Falster Fm may indicate sylvinite (KCl) or high concentrations of feldspar.

Figure 33 Photograph of cuttings from the Bunter Sandstone Formation at 1232 m (4045') showing domination of mm-sized quartz grains. The sample also has a high Si content and a high Si/Al ratio, and an overall chemical composition interpreted to be dominantly composed of quartz. Grey lid shown to the right have a diameter of 45 mm.

The calculated API response of the cuttings (SGR) based on the HH-XRF determination of K, U and Th are in generally good agreement with the measured GR log curve in the borehole (Figure 32). In general, it appears that the API of the cuttings plot with slightly deeper depths the equivalent GR log probably representing a "lack time" reflecting a poor depth control of the cuttings. The API values in Rødby-1 well range up to 60 in the Ørslev and lower part of the Bunter Sand Formation. This is about 40 API units lower compared to what is typical measured in the Fjerritslev Formation (c.f. Figure 26).

The low GR readings in the Falster Formation between 880–960 m correspond to the presence of carbonate whereas the above and below lying anhydrite appears to have medium high GR responses. In the Ørslev Formation the GR is low in the basal part of the formation.

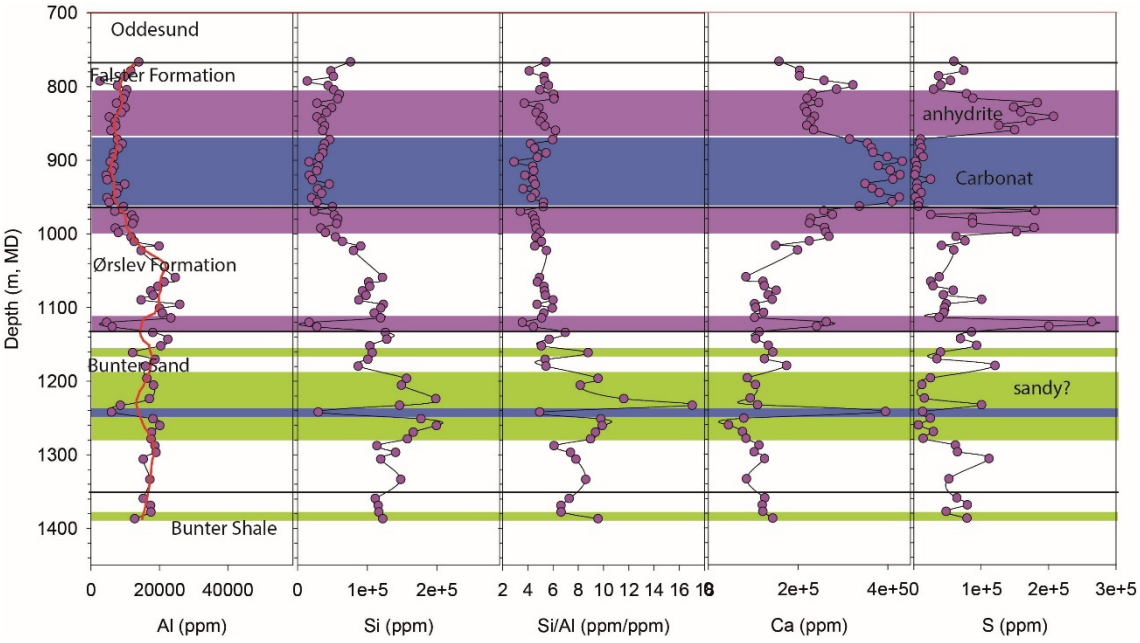

Figure 34 Elemental logs of Al, Si, the Si/Al ratio, Ca and S in the Rødby-1 well. The dominantly lithology (anhydrite - pink, carbonate - blue, sandy - yellow) is interpreted from HH-XRF data. Sandy beds are interpreted with a Si/Al ratio > 8. Red curve in Al diagram is the LOWESS smooth trend.

Elemental logs are shown in Figure 34. The Si level has an overall high in the Bunter Sand Formation between 1190–1280 m representing the thickest sand in the formation. In this interval the Si/Al are above 8 with peak values of 17 in 1232 m (base depth of cuttings interval). The Al content has an overall high level in the lower to mid part of the Ørslev Formation from here it decreases to low values in the carbonaceous and anhydritic Falster Formation (Figure 34).

The carbonaceous and anhydritic nature of the Falster Formation can be seen from the Ca-S relationship as anhydrite samples have medium high Ca and S whereas carbonaceous samples only have high Ca (Figure 34).

The K/Al ratio range between 0.5 and 1.7 in the well i.e. much higher than seen in wells like the Vedsted-1 well (compare Figure 26 and 32). Very high ratios are seen in the Falster Formation and might indicate that other K bearing minerals than feldspars and clays such as sylvine (KCl) since the sections elsewhere contain rock salt. Rock salt is generally not expected to appear in our analysis since the samples were washed with water that would have dissolved the minerals. No elevated Cl levels are thus observed in the well but as this element are generally poorly determined (se Section 3) we cannot exclude this.

The TOC content is extremely low, ranging from 0.03–0.28 wt% in the Ørslev Formation and only from 0.02–0.10 wt% in the Falster Formation (Figure 35). The lowest of these values are close to the detection limit of the Leco analyzer indicating the primary seal section is very organic-lean.

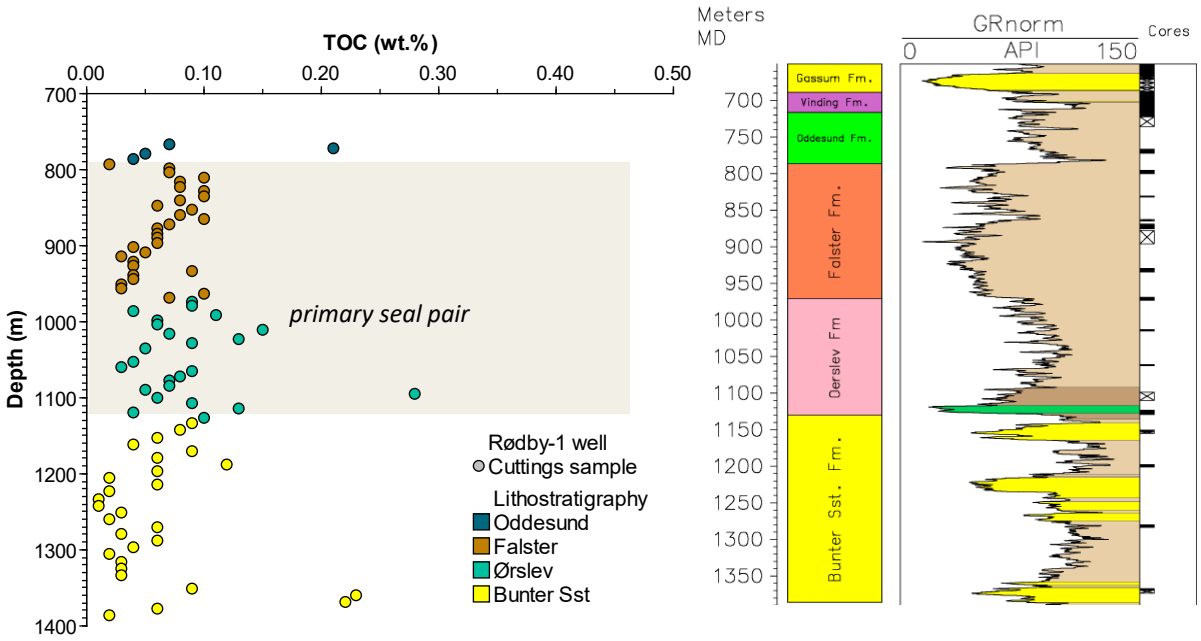

Figure 35 TOC content of the Ørslev and Falster seal section in the Rødby-1 well.

Summary

The Si level is generally high in the Bunter Sand Formation between 1190-1280 m representing the thickest sand in the formation. In this interval the Si/Al ratio is above 8 with a peak value of 17 in 1232 m (base depth of cuttings interval). The sealing sections to the Bunter Sand Formation is composed of the Ørslev and Falster formations that appear to have very different elemental composition. The mid part of the Ørslev Formation is the most clay rich parts as this section has the highest Al content. The upper part of the Ørslev and the Falster formations are carbonaceous and anhydritic. Falster Formation with possible also occurrence of rock salt as indicated by high K/Al ratios. Combined the Ørslev and Falster seal complex constitute together a 343 m thick sequence with a negligible organic matter content. Both parts are favourable for seal integrity.

4.9 Søllested-1 well

The Søllested-1 was spudded 27th of October 1982. No cores were cut. The available material was deemed insufficient for HH-XRF measurements. 120 cuttings samples were photographed (IMG0764–IMG0876) between 880–1755 m encompassing the Gassum, Vinding, Oddesund, Tønder, Falster, Ørslev and Bunter Sandstone formations.

The colour of the cuttings of the different formations in Søllested-1 (Figure 36) is generally in alignment with what is observed in the Rødby-1 well (section.4.8) .

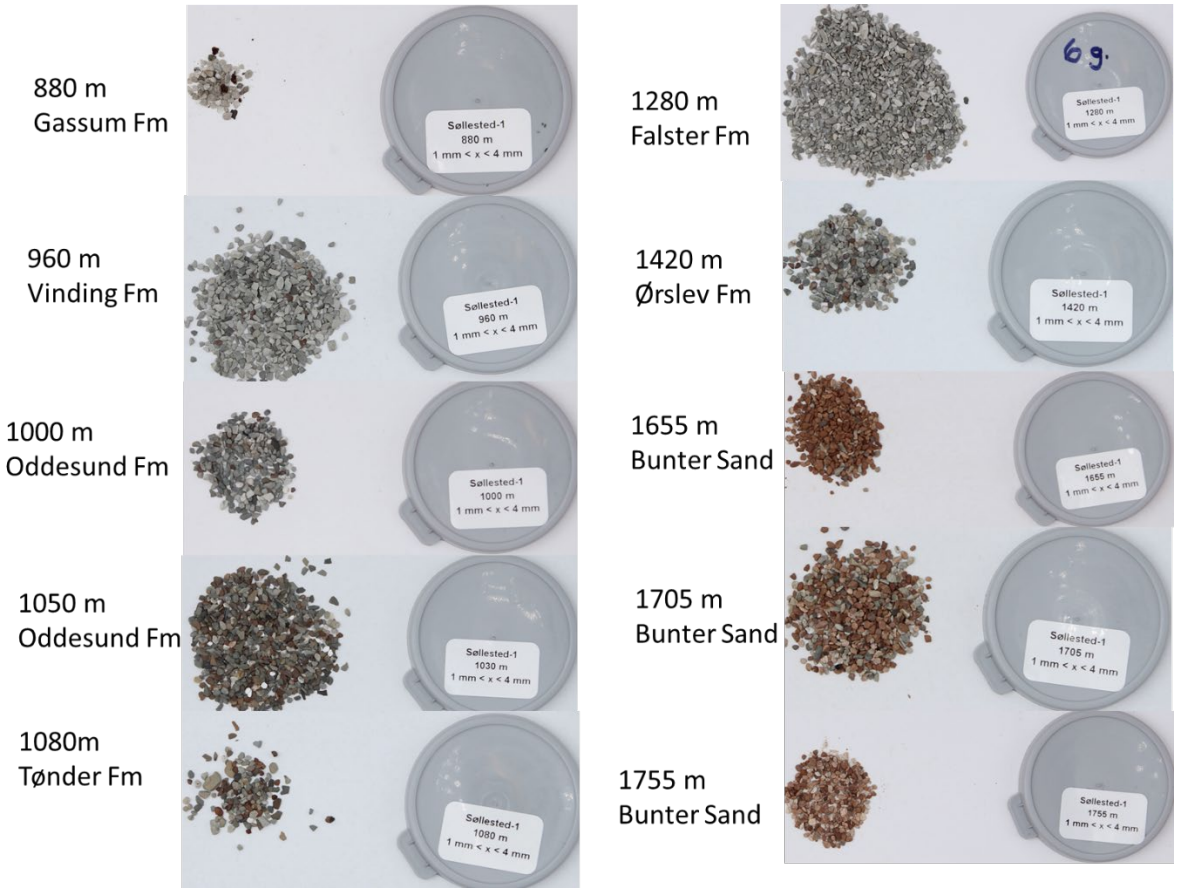

Figure 36 Selected images of the 1—4 mm cuttings fraction from the Søllested-1 well. Grey lids with marked sample size in g shown to the right have a diameter of 45 mm.

Comparable to the Rødby-1 well, the TOC content in the primary seal section (Ørslev and Falster formations) is very low (Figure 37), averaging 0.05 wt% in both formations. Minimum values down to 0.02–0.03 wt% is close to the detection limit of the Leco instrument.

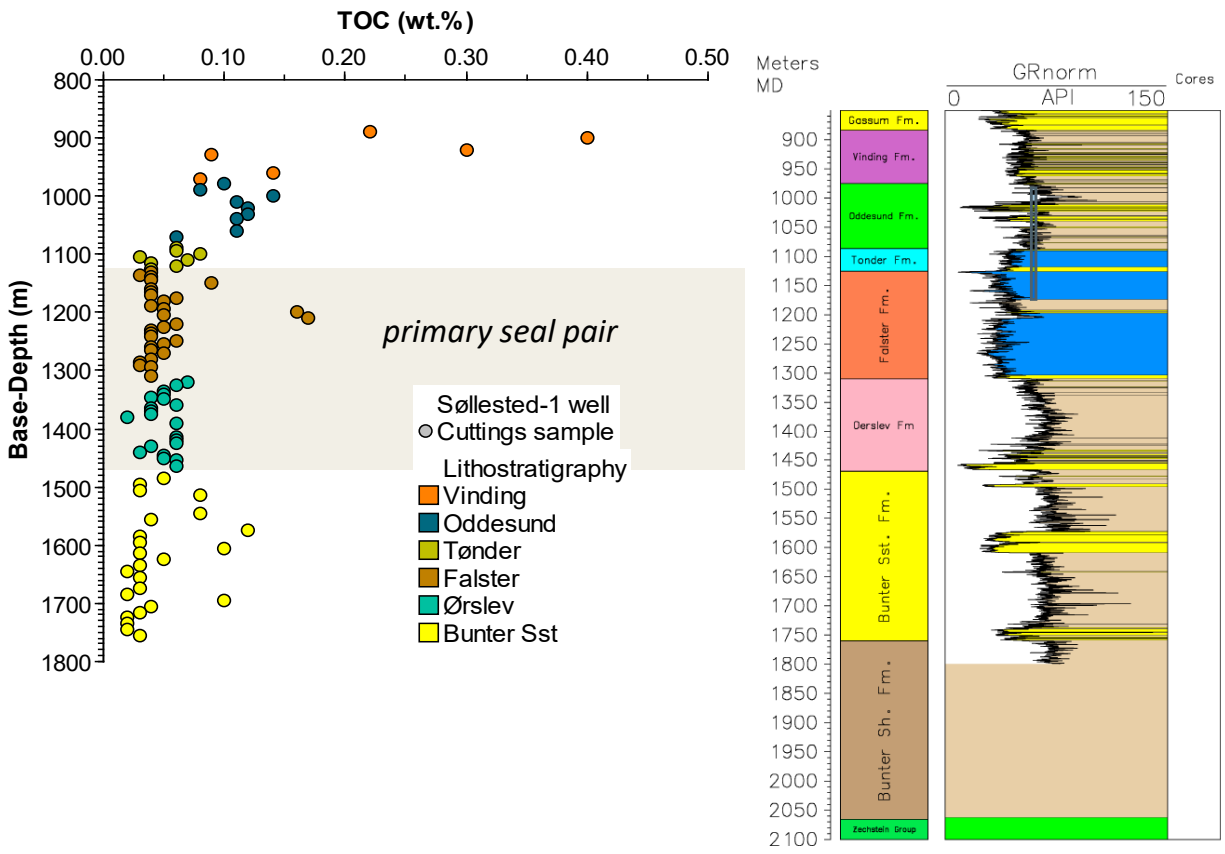

Figure 37 TOC profile in the Søllested-1 well.

Summary

Thick seal complex consists of 159 m Ørslev Formation and 184 m Falster Formation, thus amounting to a total thickness of 343 m very organic-lean mudstone section. This is considered favourable for the seal integrity.

4.10 Nøvling-1 well

The Nøvling-1 well was spudded on the 13th of September 1966. No cores were cut. 29 HH-XRF measurements (#1110–1182) and 29 cuttings images (IMG_0707–IMG_0736) was recorded between 1496–1935 m (4840'–6320') encompassing the Børglum, Fjerritslev and Gassum formations.

The cuttings from the Fjerritslev Formation range in colour from slightly multicoloured (grains being red, orange, light green and dark green) in the upper part of the Fjerritslev Formation to more homogeneous coloured dark green in the lower part of the formation (Figure 38). We also note a tendency for the multicoloured cuttings to be of generally low sample volume and the single coloured to have high weight (>15g) (Figure 38).

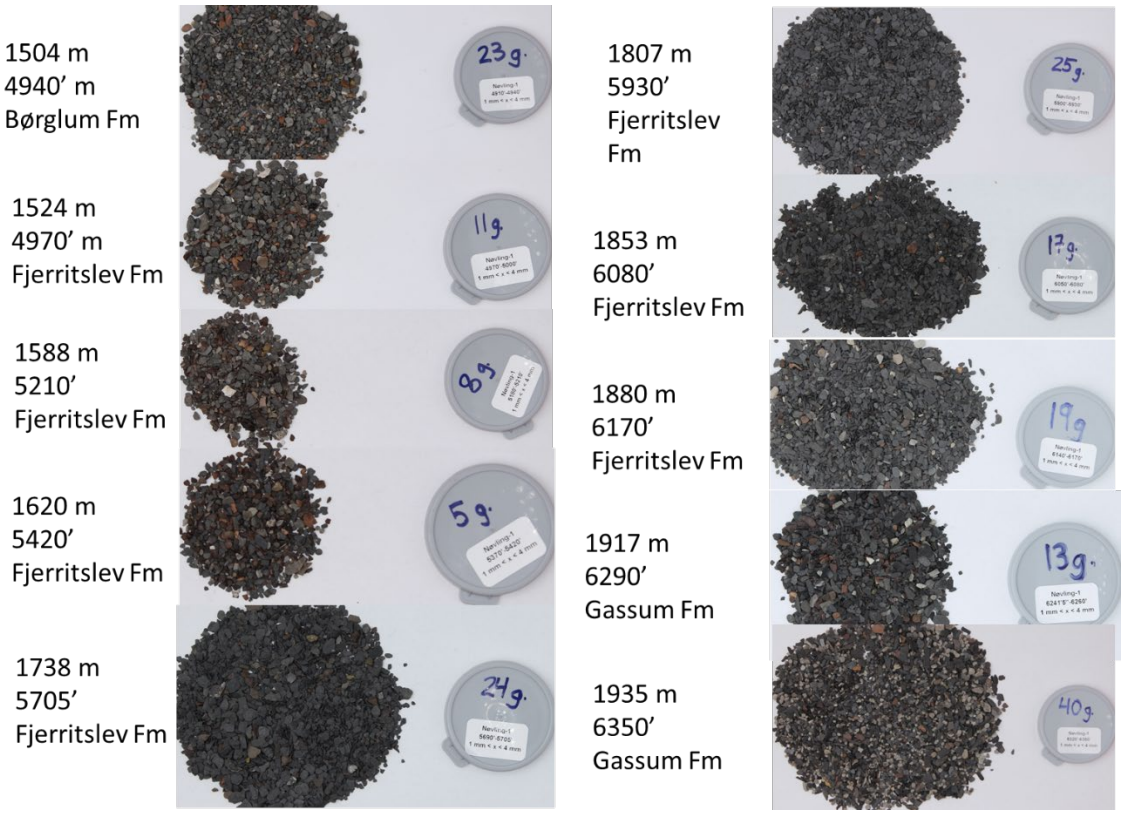

Figure 38 Selected images of the 1—4 mm cuttings fraction from the Nøvling-1 well. Grey lids with marked sample size in g shown to the right have a diameter of 45 mm.

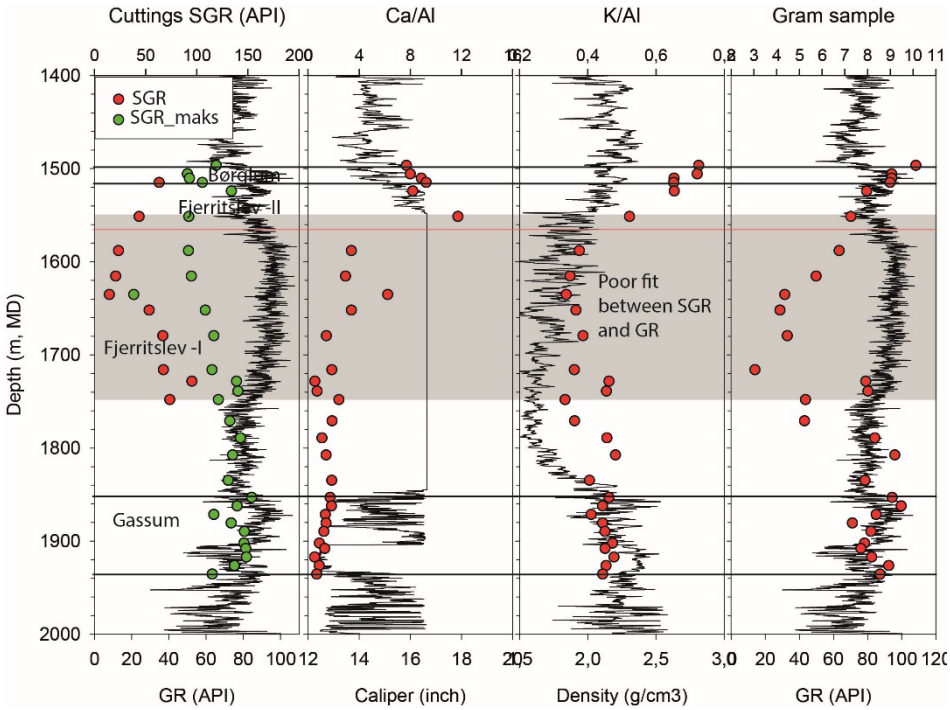

Figure 39 GR, caliper and density wireline logs plotted together with API values calculated from cutting samples based on HH-XRF data (SGR and SGR_max), the Ca/Al, K/Al ratio and sample size in the Nøvling-1 well. The grey coloured interval c.1550–c.1750 highlight an interval with poor fit between SGR and the GR wireline recordings.

The wire-line logs and selected HH-XRF data is show in Figure 39. The SGR and SGR_max deviates from each other from the top and down to c.1750 m reflecting that the U is below detection limit in the upper part of the well. In this interval there is a very distinct misfit between SGR and GR (Figure 39) as both the SGR and SGR_max fails to reproduce the generally high GR levels recorded by the wire-line GR tool (Figure 39). We also note that in the same interval where the misfit between SGR and GR is observed, the cuttings weight falls below approximately 6 g, with the lowest sample weight of 3 g around 1710 m. In the same interval there is what appears as a typical digitalisation error of the original paper version of the calliper log so that the information of the hole conditions is not known. The Nøvling-1 FWR does not mention any log breaks and the section is reported to have been drilled without any problems.

The misfit observed in the Nøvling-1 well between SGR and GR is similarly to what we have observed in other wells, most notably in the J-1X well (see Figure 21). Albeit the low sample weight, we do not suspect that the low SGR in the interval down to 1750 m is an artefact due to poor measurements since the test of analytical precision and sample weight indicate that 2 g is sufficient for stable analysis, with 5 g as the norm (see Section 4.2). Also, for many samples, the actual weight was much higher (see notes on grey lids in Figure 37), allowing the operator to take only a subset for most samples. However, for the interval with low sample weight, the operator exhausted the 1–4 mm size fraction hence these samples originally had a poor yield.

The misfit between SGR and GR could have resulted from a similar situation invoked for the J-1X, implying that the samples from the upper part of the Fjerritslev Formation have preferentially lost uranium-rich material, likely related to soft clays (possibly smectite), either during the drilling process or subsequently during sample preparation. This results in both low SGR and poor cuttings yields. In the Gassum-1 well we also invoked a similar explaination to explain why cemented parts of the formation was preferentially present in the cutting fraction. Here we also had low sample yields.

To verify this hypothesis in the Nøvling-1 well, newly prepared cuttings should be made that also aim to preserved but yet clean the soft clay cuttings, in conjunction with XRD and ICP-MS/OES analyses to determine clay types and low concentration elemental compositions. Alternatively, the mismatch between SGR and GR could be due to extensive cavings in the cuttings. In this scenario, the caved-in material, should be less radioactive than also the Børglum Fm and not being carbonate rich to explain the observed composition. The presences of such low radioactive material with enlarged holes sections could be tested by measuring the HH-XRF composition higher up in the section and / or by examining the GR and caliper log in the full well.

Elemental logs are shown in Figure 40. Si/Al ratios >8 is recorded in the Børglum Formation where also high K/Al ratios have been recorded (Figure 39) suggesting coarser beds probably felspathic. In the Gassum Formation, no sudden shifts in the Si/Al ratio is observed (Figure 40). In the interval GR log lows have been interpreted to reflect sandstones and the lack of sensitivity in the Si/Al ratio might as have been suggested for other wells reflect the analysed sample size fraction of the HH-XRF that leads to over-representation of the shaly component of the Gassum Formation.

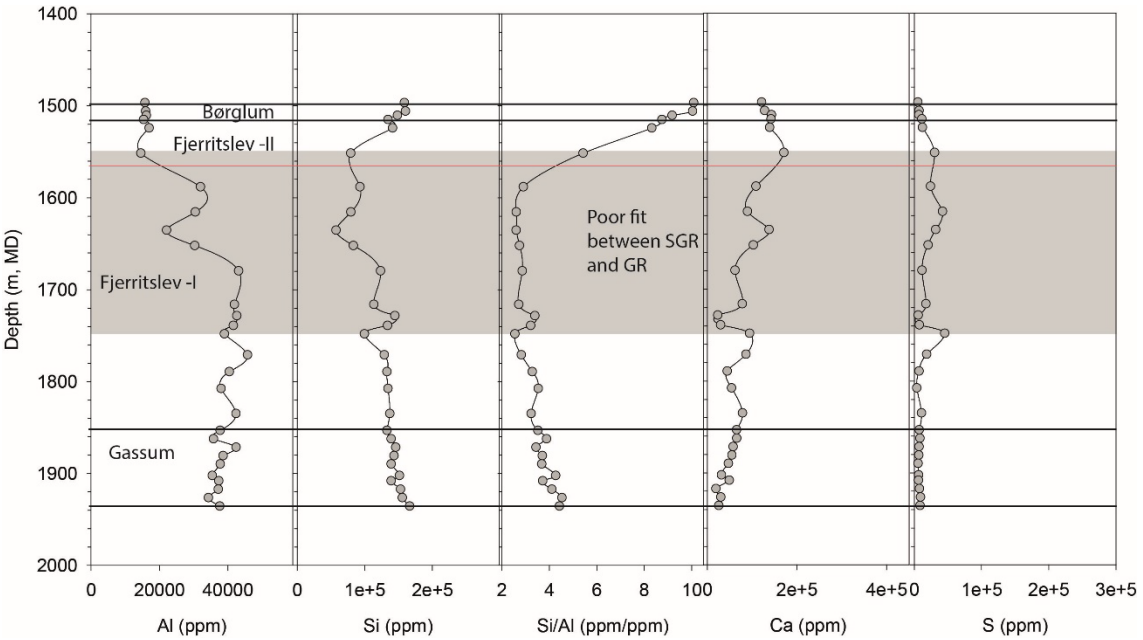

Figure 40 Elemental logs of Al, Si, the Si/Al ratio, Ca and S from the Nøvling-1 well.

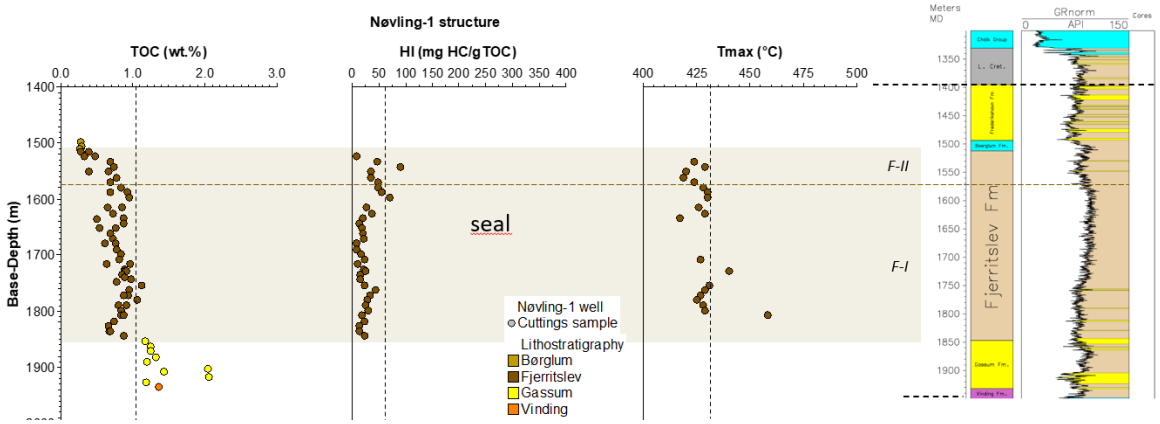

Figure 41 TOC, HI and Tmax in the Nøvling-1 well.

Summary

The Gassum Formation in the Nøvling-1 well is seal by 335 m thick Fjerritslev Fm mudstones (275 m F-1 Member + 60 m F-II Member) plus 18 m Børglum Formation mudstones. Samples and log do not indicate sandy beds in Fjerritslev Formation. Cuttings is interpreted to reflect the Fjerritslev Formation in the deeper parts and can be used to characterise the seal capacity. Cuttings from the upper parts of the formation requires more studies to documents its validity as seal. Low TOC content fluctuating between only 0.28–1.12 wt% (mean: 0.76 wt%). Hydrogen Index (HI) is very low with a maximum HI of only 91 mg HC/g TOC and a mean of 28 mg HC/g TOC. A mean Tmax of 429 °C indicates the organic matter is thermally immature. Thick mudstone with low content of dispersed, thermally immature, and overall inert organic matter is favourable for the seal integrity.

5. Discussion

In several wells, petrophysical logs and cuttings sampkes are the only information available from the subsurface. The accuracy of cutting samples in representing the subsurface is crucial. To reduce potential errors, we took several steps in the cutting preparation process, including washing the samples to remove drill mud and adhering to a well-established preparation procedure that includes sieving, specifically using the 1-4 mm size fraction to limit the influence of cavings. This also involved testing for sample size and reproducibility of standards over time. Despite these efforts, the comparison of the HH-XRF data with wireline log readings and interpreted subsurface lithologies leaves little doubt that the cuttings we have analyzed are all influenced by sampling errors related to the drilling process, handling at the drill site, laboratory preparation, and finally, the measurement itself (c.f. Figure 42).

From the cuttings imaging, it is clear that samples from the reservoir contain uncemented large quartz grains but are mostly composed of shaly rock fragments, likely representing interbedded finer beds evident from the wireline log signatures. However, by choosing to work with only the 1–4 mm size fraction for the HH-XRF samples, we may have inadvertently removed unconsolidated finer sand grains from our samples and tended to overrepresent hardened mudstone versus soft mudstone and diagenetically cemented beds, as well as giving an undue advantage to pyrite and carbonate concretions in the sampling process.

At present, we cannot quantify the impact of this on the chemical composition presented and the discussion below. We only urge to keep in mind that the cuttings are largely biased towards the cemented parts of the formation and hardened mudstone. However, in future work, we aim to improve the sampling and preparation of the cuttings to minimize this effect as much as possible.

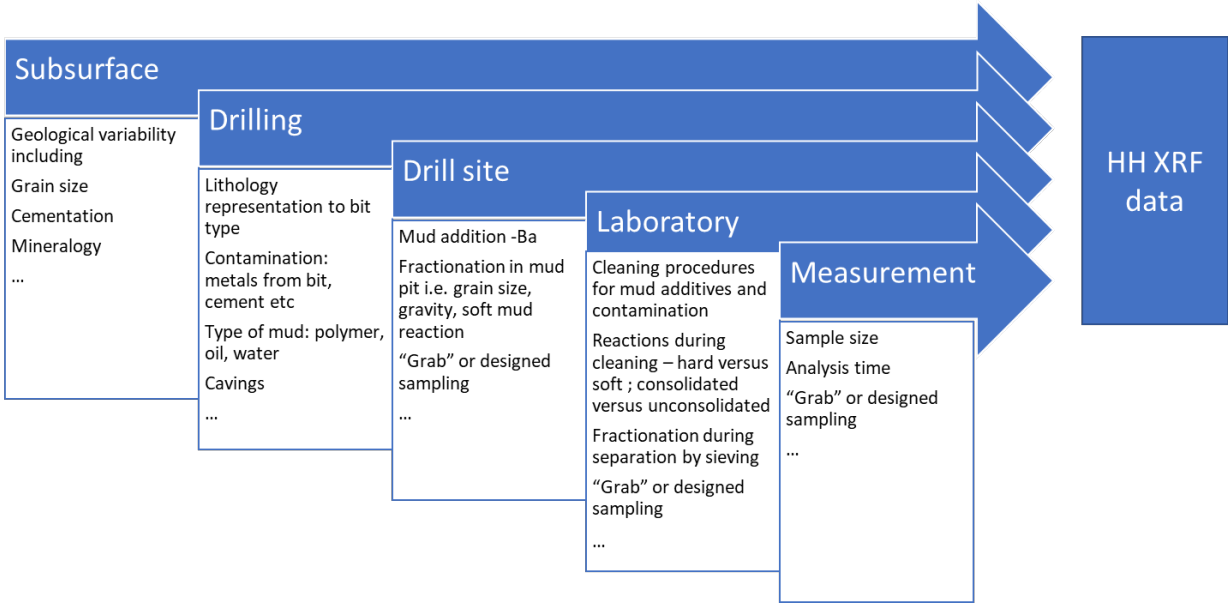

Figure 42 Factors potentially influencing the real rock composition in the subsurface (our object) and the obtained HH-XRF data leading to sampling errors with respect to representation of the subsurface.

5.1 Triassic and Jurassic seal types

The geochemical data, presented on a well-by-well basis, are collectively illustrated in Figure 43 to highlight the differences and similarities between the Triassic and Jurassic strata in Eastern Denmark. Generally, Figure 43 shows that the Upper Triassic to Jurassic samples (Gassum and Fjerritslev fms) from J-1X, Vedsted-1, Gassum-1, Nøvling-1, and Fjerritslev-2 cluster together,

while samples from Rødby-1, representing the Lower to Mid/Upper Triassic Bunter sand, Ørslev, and Falster formations, plots separately. This distinction is most evident in the K vs. Al and Fe vs. S diagrams.

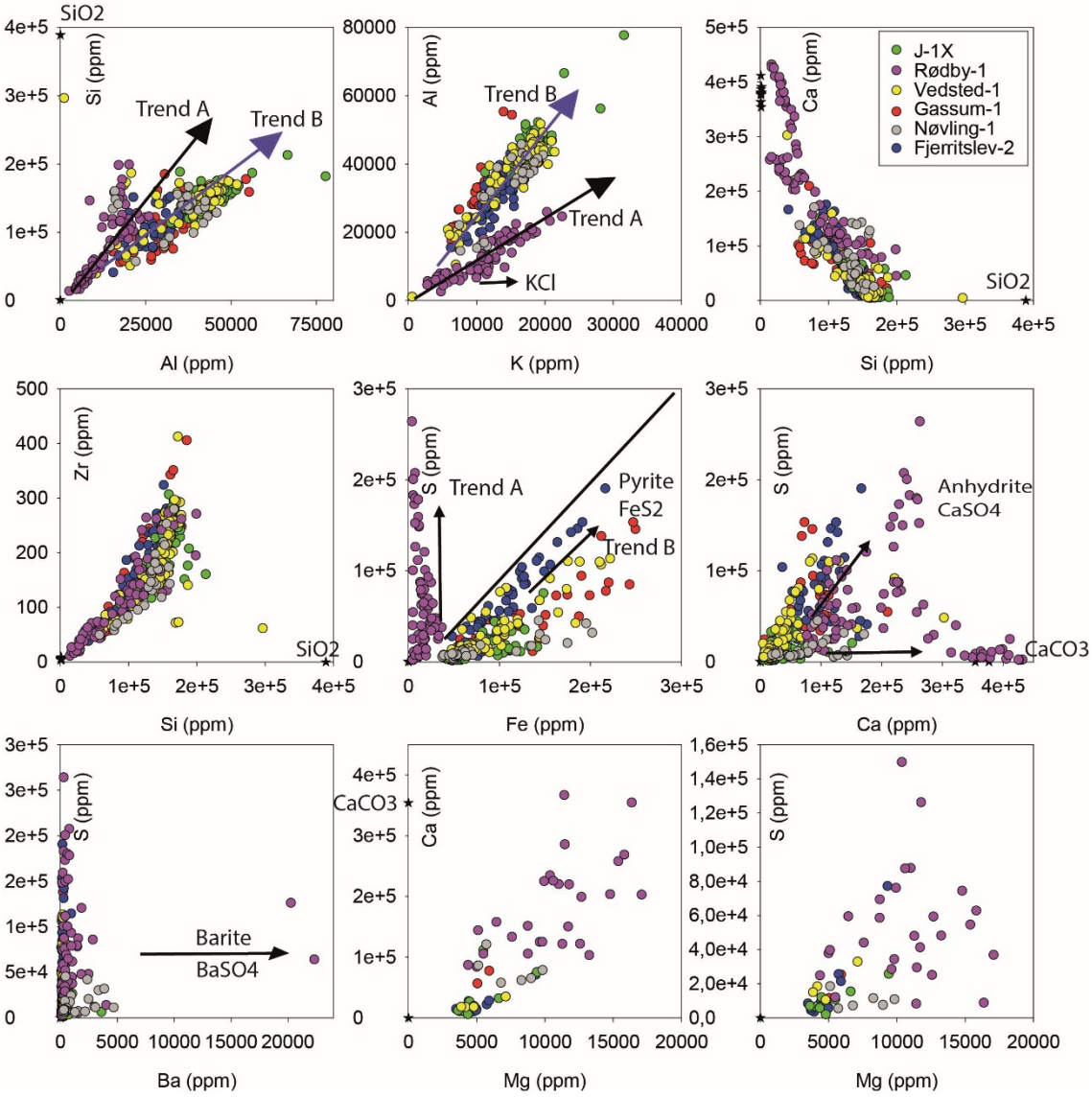

Figure 43 Cross-plot of HH-XRF determined element concentrations. The Gassum and Fjerritslev fms generally follow trend line "B" and the Bunter, Ørslev and Falster fms follow Trend line "A".

The K vs. Al diagram (Figure 43) serves as a useful discriminant for the mineralogy of detrital phases, as the Al/K ratio differs significantly between feldspar (low) and clay minerals such as mica, illite, smectite, and kaolinite (the latter two of which do not include K), with kaolinite having the highest ratio. Thus, this diagram reflects a feldspar-rich Lower to Mid/Upper Triassic suite versus a more clay-rich suite composed of samples from the Gassum and Fjerritslev formations. The Fe vs. S diagram is adept at distinguishing between terrestrial/oxic and marine/anoxic environments, as a positive correlation indicates the presence of pyrite, which forms in reducing marine environments. In this diagram, samples from Rødby-1 show no clear relationship with Fe, whereas the other wells generally display a positive correlation with Fe, suggesting that S is associated with Fe, most likely in the form of pyrite (Fe_2S). On the other hand, the Rødby samples

exhibit a positive relationship between S and Ca, suggesting that the S-rich samples contain anhydrite ($CaSO_4$) instead of pyrite.

Rock typing by multivariate data analysis

Principal component analysis (PCA) was conducted on the HH-XRF data to explore the potential for rock typing using the entire HH-XRF dataset. The recommended data normalization method, the centered log-ratio (CLR), was applied. Corrections for false zeros were made before the analysis by assuming that levels below detection were equal to the reported analytical error.

PCA is a multivariate analytical approach that differentiates rock types not by their sedimentary facies, which are dependent on depositional processes, but rather by their functional properties, in this context, their chemical composition. The PCA model transforms a matrix of measured values into sets of projection subspaces defined by principal components. Each principal component is a linear combination of all measured variables, designed to maximize the variance and reveal interrelationships between samples and variables. The PCA-defined rock types emphasize the controlling factors of the most significant rock properties based on the full spectrum of measured parameters, not just a select few, as illustrated in Figure 44. The PCA results are visualized on a score plot showing sample relationships and a loading plot indicating parameter relationships. In these diagrams, samples, elements, and variables that plot close to each other are most similar or positively correlated, whereas those that plot further apart are dissimilar or exhibit negative correlations.

The PCA model for all HH-XRF elements deemed suitable for analysis (cf. Table 1) shows that the first three components account for 69% of the variance in the total dataset. On the first two component loadings (PC-1 and PC-2), the separation of samples from Rødby-1 from all other samples is evident on the score plot. The loading plot reveals that the main chemical differences can be attributed to high Sr, Ca, and S content and low detrital elements. Within the other wells, the samples plot between endpoints defined by J-1X, leaning towards more "clay", and Gassum-1, leaning towards more "sulfide". This may be attributed to a finer-grained nature of the J-1X among all Fjerritslev analysis wells, as it plots with higher normalized Th, Rb, and Zr than other samples. The affinity of the Gassum-1 sample to more cemented parts, i.e., higher Fe, S, Mn, and Zn is judged more to reflect biases in sample preparation that led to the concentration of these more cemented parts of the mudstone rather than reflecting a special "Gassum-1" subsurface rock type.

The PC component 3 further details the Zn-Mn relationship. Here it is evident that Zn has affinity to S i.e. sulphides associated with pyrite and that Mn represent a different component likely a carbonate phase.

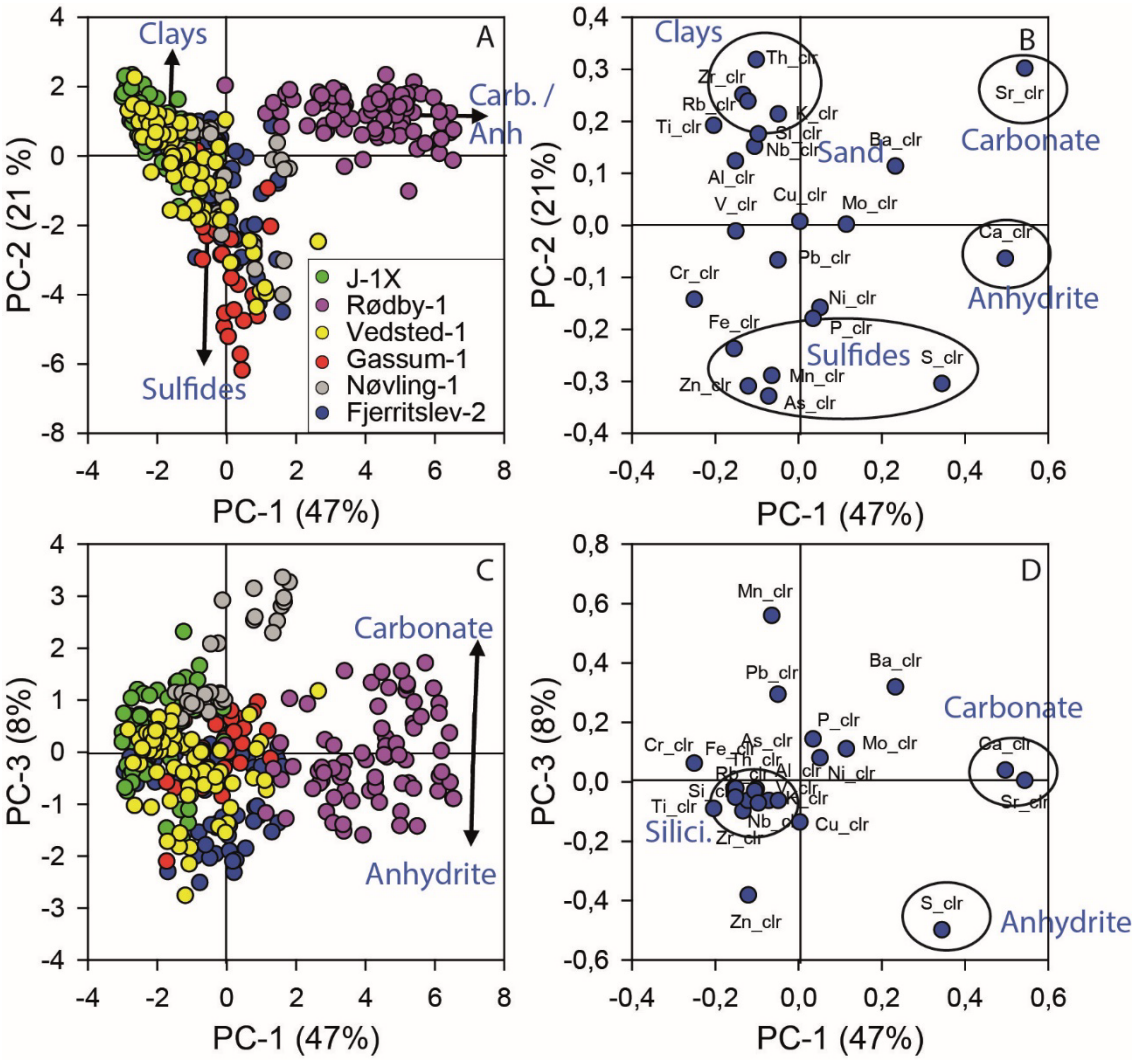

Figure 44 PCA model of the HH-XRF determined element concentrations (see Table 1). The subscript "_clr" indicate that the dataset was central log ratio normalised prior to analysis.

6. Summary of Reservoir – Seal pairs characterisation

Seal capacity of the Fjerritslev Fm

The technical report on the seal capacity of the Fjerritslev Formation as investigated by Springer et al. (2020) and Gregersen et al. (2023), highlights its significant potential for sealing, particularly in the context of carbon capture and storage (CCS). The Fjerritslev Formation, investigated primarily in the Stenlille area, features here a seal succession approximately 250–300 meters thick, characterized by interbedded porous sandy-silty layers within the F-Ia member. This division results in both lower and upper seal units, with the upper part deemed exceptionally effective for sealing purposes. Key findings include an average porosity of 11%, air-permeability of 160 µD, and *in-situ* liquid permeability in a massive mudstone layer reaching 3 nD; comparable to the best-known petroleum caprocks. Additional overburden measurements indicated liquid permeabilities around 200 nD, underscoring the formation's excellent seal quality, which has been validated by over 30 years of natural gas storage in the underlying Gassum Formation.

Capillary entry pressure, a critical factor for assessing seal capacity, was assessed from Mercury Injection Capillary Pressure (MICP) experiments. Despite the challenges in converting results from the mercury/air system to the CO_2/brine system, due to differences in contact angle and interfacial tension, standard conversion values suggest capillary entry pressures ranging from 5–10 MPa, with recent measurements indicating a lower range of 1–5 MPa. The buoyancy force exerted by the CO_2 on the caprock, influenced by the density difference between formation water and injected CO_2, dictates the seal capacity for CO_2 storage. Estimations show that the caprock can support CO_2 column heights ranging from approximately 290 m to over 1000 meters. Although further data from the Fjerritslev Formation are needed, preliminary assessments confirm its excellence as a primary seal for the Gassum Fm, possessing robust sealing capabilities.

<u>Comparison with the Stenlille area</u>

No HH-XRF data have been collected from the Stenlille wells, from which the good seal properties cited above have been established. However, similar good seal properties have been measured in the Vedsted-1 well (Mbia et al., 2014), as also noted by Springer et al. (2020) in their review. The cuttings chemistry in the Vedsted-1 well appears to be similar to that of other studied Fjerritslev wells (c.f. Figures 43 and 44), and it seems reasonable to suggest, as a first approximation, that these wells share the same good seal properties. At the very least, we can safely conclude that the HH-XRF analyses do not in any way diminish the potential of the Fjerritslev seal properties in the Gassum-1, Fjerritslev-2, J-1X, and Nøvling-1 wells.

The clay content in the Vedsted-1 well ranges between 40–45% within the 1350–1745 m interval (7 samples) studied by Mbia et al. (2014). This interval exhibits a Si/Al ratio of 4 and an Al content of about 4000 ppm or slightly higher (Figures 43, 44). Smectite and kaolinite may constitute up to 50% of the clay volume in Vedsted-1, a significant portion of which will go undetected by the GR curve, as these clay types are non-radioactive due to their lack of potassium (K), thorium (Th), and uranium (U) - although smectite might potentially include surface-bound U and K if part of it occurs in mixed-layer illite/smectite. A similar K/Al trend, as observed in Vedsted-1, can also be seen in the Gassum-1, Fjerritslev-2, J-1X, and Nøvling-1 wells, suggesting that a similar clay mineral assemblage is likely present in these wells as well.

Seal capacity of the Lower to Middle Triassic Formations

The seal capacity of the Lower to Middle Triassic formations has not received similar attention as the Fjerritslev Fm. In addition, whereas the Fjerritslev Formation was deposited in a humid climate under dominantly fully marine conditions, the Lower to Middle Triassic formations, including the Bunter Sand, Ørslev, and Falster formations, were deposited under arid to semi-arid

climatic conditions with localized restricted marine to playa lacustrine evaporitic conditions. This makes drawing parallels between them very challenging.
Geochemically, the units are also markedly different. The Al content in the Rødby Formation reach up to 2000 ppm, which is significantly lower than in the Vedsted-1 wells, suggesting that the clay volume is much less than the 40% recorded here (Mbia et al., 2014). Similarly, the Si content is lower, indicating an overall low detrital content in the Triassic seal formations. The Bunter, Ørslev, and Falster formations all have low K/Al ratios, indicative of the presence of feldspars. This aligns with the findings of Weibel et al. (2017), who found that K-feldspars and micas in arid to semi-arid conditions were largely unaltered, whereas under humid conditions, they were largely replaced by kaolinite. This process may be part of the explanation for the difference in K/Al ratio observed in Figure 43. In addition, the units contain interbeds of anhydrite and limestone and possible also rock salt due to high K/Al ratios, although rock salt has not been observed in the Rødby-1 well.
In summary, the good seal capacities with respect to CO_2 storage that have been inferred for the Jurassic Fjerritslev Formation cannot be directly applied to the Lower to Middle Triassic formations. However, this does not mean that these formations lack good seal capacity. On the contrary, the heterogeneous nature of the formation might lower the risk for leak, as suggested by Bruno et al. (2014) since fracture propagation through heterogeneous strata can be anticipated to be much more complex due to the differences in competence between the beds. Additionally, if presence rock salt will also enhance the seal capacity due to its very low entry pressures and its self-healing nature towards fractures.

6.1 Recommendations for further studies on seal capacity

Site-specific studies on the seal capacity are needed for all structures to be matured towards CO_2 storage. For the Bunter Sand Formation in the Rødby structure, which is primarily sealed by the fine-grained parts of the Bunter Sand, the Ørslev, and the Falster formations, the need to establish fundamental knowledge of the seal properties is very high. This is because we cannot draw parallels to the better-known Fjerritslev Formation as we can for many of the Gassum–Fjerritslev reservoir-seal pairs that are under exploration elsewhere in Denmark.
In Figure 3, a workflow to establish the fundamental seal information is outlined. In this workflow, the studies conducted here, i.e., HH-XRF, cuttings imaging, and TOC and Rock Eval analysis, form only part of the screening data that needs to be gathered. Other important high-volume samples include porosity, surface area determination, mineralogy, and clay type determination combined with grain size analysis. Once established, selection for more costly but crucial analyses such as pore size distribution and capillary entry pressures, as well as petrography and microfacies descriptions, is advised.
Calibration of the HH-XRF measurements by ICP-MS and ICP-OES and X-ray diffraction to support interpretation of chemical composition.

7. Conclusions

To evaluate the seal integrity direct measurements and tests to gauge the rock properties are needed. In Denmark, the onshore wells were mainly drilled in the 1950-1980'ies and many of the old wells have no wire-line log data or very poor data when compared to modern standards. In addition, cores of the seal section were rarely taken and the only source of material for full formation evaluation of the seal integrity are in most cases cuttings samples.

Our study of the feasibility of using cuttings for evaluation the seal capacity has shown that the cuttings are largely biased towards the cemented parts of the formation and hardened mudstone. However, by comparing the GR logs respond to the API values measured on cuttings intervals where cuttings adequately represent the subsurface can be identified.

In future work, we aim to improve the sampling and preparation of the cuttings to minimize the bias effect as much as possible. This includes:

To analyse all size fractions of eth cuttings.

To analyse U, Th and K with ICP-MS/OES to enhance the analytical quality and thus to allow a better comparison between SGR and the GR curve for determination of the representativeness of the cuttings.

To separate the cuttings samples into sand and mudstone fraction and to conduct measurements hereon to examine the range in API between the lithologies.

To preform quantitative analysis of the cutting's images with tools such as ImageJ to extract more information, such as downfall of different coloured fragments.
Calibration of the HH-XRF measurements by ICP-MS and ICP-OES.

Identify mineralogy and petrography of all cored intervals and supplement that with cuttings samples where core samples are lacking.

8. Acknowledgements

We thank the CCS 2022–24 project for funding and Annette Ryge and Ditte Kiel-Dühring for sample preparation and analysis. The cuttings were photographed during the period from October 31st to November 3rd, 2022, by Victor Chamoux, Noé Nguyen, Héloïse Jamet and Colin Debonnet all visiting students from University of Unilasalle, France. We thank Finn Mørk and Rikke Weibel for discussion of the finding in this report and specifically Rikke Weibel for providing an internal review of the report. The organic geochemistry depth plots were created with the pIGI-3 software kindly provided by Integrated Geochemical Interpretation Ltd.

9. References

Bordenave, M.L., Espitalié, J., Leplat, P., Oudin, J.L., Vandenbroucke, M., 1993. Screening techniques for source rock evaluation. In: Bordenave, M.L. (Ed.), Applied Petroleum Geochemistry. Éditions Technip, Paris, pp. 219–278.

Bruno, M.S., Lao, K., Diessl, J., Childers, B., Xiang, J., White, N., van der Veer, E. 2014. Development of improved caprock integrity analysis and risk assessment techniques. Energy Procedia 63, 47084744.

Doornenbal and Stevenson, 2010. Petroleum geological atlas of the southern permian basin area (SPBA). TNO Geological Survey of the Netherlands ; European Association of Geoscientists & Engineers (EAGE), Utrecht, Houten, the Netherlands.

Folk, R.L., Andrews, P.B., Lewis, D.W., 1970. Detrital sedimentary rock classification and nomenclature for use in New Zealand. New Zealand Journal of Geology and Geophysics, 13, 937–968.

Lafargue, E., Marquis, F.D.S., Pillot, D., 1998. Rock-Eval 6 applications in hydrocarbon exploration, production, and soil contamination studies. Revue de l'Institut Francais Du Petrole 53, 421–437. doi.org/10.2516/ogst:1998036

Gregersen, U., Vosgerau, H., Smit, F.W.H., Lauridsen, B.W., Mathiesen, A., Mørk, F., Nielsen, L.H., Rasmussen, R., Funck, T., Dybkjær, K., Sheldon, E., Pedersen, G.K., Nielsen, C.M., Bredesen, K., Laghari, S., Olsen, M.L., Rasmussen, L.M., 2023. The Havnsø structure. Seismic data and interpretation to mature potential geological storage of CO_2. Danmarks og Grønlands Geologiske Undersøgelse Rapport 2023/38. https://data.geus.dk/pure-pdf/GEUS-R_2023-38_web.pdf

Mbia, E.N., Fabricius, I.L., Krogsbøll, A., Frykman, P., Dalhoff, F., 2014. Permeability, compressibility and porosity of Jurassic shale from the Norwegian–Danish Basin. Petroleum Geoscience, Vol. 20, 2014, pp. 257–281.

Nielsen, L.H., 2003. Late Triassic–Jurassic development of the Danish Basin and Fennoscandian Border Zone, Southern Scandinavia. In: Ineson JR, Surlyk F, editors. The Jurassic of Denmark and Greenland. Geological Survey of Denmark and Greenland Bulletin 1; 2003. p. 459–526.

Petersen, H.I., Nielsen, L.H., Bojesen-Koefoed, J.A., Mathiesen, A., Kristensen, L., Dalhoff, F., 2008. Evaluation of the quality, thermal maturity and distribution of potential source rocks in the Danish part of the Norwegian-Danish Basin. Geological Survey of Denmark and Greenland Bulletin 16, 66 pp.

Schovsbo, N.H., Nielsen A.T., Harstad, A.O., Bruton, D.L., 2018. Stratigraphy and geochemical composition of the Cambrian Alum Shale Formation in the Porsgrunn core, Skien-Langesund district, southern Norway. Bulletin of the Geological Society of Denmark 66, 1–20.

Schovsbo, N.H., Petersen, H.I., Weibel, R., Springer, N. 2022. Upper seal characterisation and capacity evaluation based on cutting analysis of the Nini-4 well. Project Greensand Phase 2 W3.7 report. Danmarks og Grønlands Geologiske Undersøgelse Rapport 2022/31 https://doi.org/10.22008/gpub/34666

Schovsbo, N.H., Weibel, R., Springer, N., Fodgen, A., Sheldon, E., Petersen, H.I., 2023. Workflow for characterization of the Nini West storage site seal, Danish North Sea. EAGE GET conference November 2023. https://doi.org/10.3997/2214-4609.202321010

Springer, N., Dideriksen, K., Holmslykke, H., Kjøller, C., Olivarious, M., Schovsbo, N., 2020. Capture, Storage and Use of CO2 (CCUS). Seal capacity and geochemical modelling. GEUS Rapport 2020/30 42 p. https://doi.org/10.22008/gpub/34527

Weibel, R., Olivarius, M., Kristensen, L., Friis, H., Hjuler, M.L., Kjøller, C., Mathiesen, A., Nielsen, L.H., 2017. Predicting permeability of low-enthalpy geothermal reservoirs: A case study from the Upper Triassic – Lower Jurassic Gassum Formation, Norwegian–Danish Basin. Geothermics 65, p 135-157. https://doi.org/10.1016/j.geothermics.2016.09.003

Appendix A

Results of standards.

STD	Car-bonate	Carbonate	Car-bonate	Car-bonate	Car-bonate	Car-bonate	Car-bonate	Carbonate
ppm	Middle	Median	Std	Min	Max	Range	N	Mean/Std
Al								
As								
Ba								
Bal	613072	612333	15925	585374	645642	60268	27	38.5
Ca	384120	385573	16617	343864	411987	68124	27	23.1
Cl	269	271	49	185	366	180	27	5.5
Co								
Cr								
Cu								
Fe								
K								
Mn								
Mo	6	6	2	3	9	6	27	3.9
Nb								
Ni								
P								
Pb								
Rb								
S								
Se								
Si	1140	1089	311	724	2105	1382	27	3.7
Sr	74	73	13	51	97	46	27	5.9
Th								
Ti								
U								
V								
Zn								
Zr	5	5	2	3	9	6	22	3.2

STD	180-673	180-673	180-673	180-673	180-673	180-673	180-673	180-673
ppm	Middle	Median	Std	Min	Max	Range	N	Mean/Std
Al	42388	42082	1366	39886	45470	5584	27	31.0
As	39	39	7	28	57	29	26	5.3
Ba	866	865	30	803	917	115	27	28.4
Bal	592853	593904	5709	577839	602023	24184	27	103.8
Ca	4712	4733	119	4426	4957	531	27	39.4
Cl	287	244	169	90	917	827	26	1.7
Co								
Cr	79	79	10	60	101	41	27	8.1
Cu	251	250	11	231	268	37	27	23.7
Fe	31010	31007	340	30372	31826	1454	27	91.3
K	24984	25009	250	24205	25351	1146	27	99.8
Mn	5498	5562	204	4987	5740	752	27	27.0
Mo	18	17	2	14	22	8	27	7.7
Nb	33	33	2	29	38	9	27	19.2
Ni	57	58	9	35	80	45	27	6.4
P	881	856	112	651	1082	431	27	7.8
Pb	980	977	40	897	1057	160	27	24.5
Rb	137	137	2	132	142	10	27	57.1
S	2495	2470	208	2181	3094	914	27	12.0
Se								
Si	284500	283932	5278	274515	295220	20705	27	53.9
Sr	142	143	2	139	146	8	27	66.4
Th	22	22	4	16	34	18	27	5.8
Ti	3503	3467	118	3342	3776	434	27	29.7
U	9	9	2	6	12	5	11	4.9
V	81	82	9	60	104	44	27	9.1
Zn	815	827	44	708	877	169	27	18.4
Zr	419	412	21	377	468	90	27	20.4

STD	180-661	180-661	180-661	180-661	180-661	180-661	180-661	180-661
ppm	Middle	Median	Std	Min	Max	Range	N	Mean/Std
Al	33722	33626	1564	30975	37363	6388	27	21.6
As	433	435	6	422	444	22	27	74.5
Ba	783	784	23	737	823	86	27	34.8
Bal	649081	650903	7297	635284	661866	26581	27	88.9
Ca	6181	6198	119	5893	6373	480	27	51.9
Cl	372	385	95	150	510	360	27	3.9
Co	99	87	29	70	163	93	14	3.4
Cr	521	520	10	504	537	33	27	52.8
Cu	22	22	3	15	27	12	26	6.6
Fe	18040	18014	161	17738	18317	578	27	112.1
K	11921	11935	151	11554	12161	607	27	78.8
Mn								
Mo	5	4	1	3	8	5	18	3.6
Nb	10	10	1	8	12	4	27	11.3
Ni	24	24	4	17	32	15	16	5.7
P	345	345	60	265	475	210	12	5.8
Pb	503	504	8	479	519	40	27	60.8
Rb	62	61	1	60	65	5	27	50.4
S	1071	988	178	885	1514	630	27	6.0
Se	465	467	5	455	474	20	27	89.1
Si	272957	272303	5340	263517	283629	20113	27	51.1
Sr	75	75	2	72	77	6	27	49.9
Th	10	10	2	7	14	7	26	5.4
Ti	3391	3377	79	3214	3537	323	27	43.1
U	6	5	2	4	10	5	7	3.0
V	99	99	8	84	116	31	27	12.6
Zn	34	33	3	29	43	14	27	10.4
Zr	351	352	13	319	372	53	27	27.3

STD	180-649	180-649	180-649	180-649	180-649	180-649	180-649	180-649
ppm	Middle	Median	Std	Min	Max	Range	N	Mean/Std
Al	44967	45334	2240	40983	49859	8877	27	20.1
As	10	10	1	8	11	4	26	9.5
Ba	927	931	23	871	964	92	27	41.1
Bal	645871	644332	9754	624665	664116	39451	27	66.2
Ca	20832	20937	427	20115	21776	1661	27	48.7
Cl	498	517	115	285	699	413	27	4.3
Co	152	149	32	109	202	93	17	4.8
Cr	131	141	33	86	177	92	27	3.9
Cu	37	37	4	28	46	18	27	8.2
Fe	33130	33020	380	32620	33994	1373	27	87.2
K	15792	15773	204	15435	16180	745	27	77.4
Mn	466	460	25	432	513	80	27	19.0
Mo	5	4	1	3	7	4	11	3.9
Nb	7	7	1	6	8	3	27	10.4
Ni	60	59	6	48	74	26	27	9.7
P	657	673	109	466	815	348	27	6.0
Pb	16	16	2	12	21	9	27	7.1
Rb	87	87	2	83	91	8	27	50.6
S	1513	1438	214	1252	2033	781	27	7.1
Se								
Si	225529	225733	5651	214230	234909	20680	27	39.9
Sr	211	211	3	206	216	10	27	81.0
Th	10	10	1	7	12	5	27	8.3
Ti	3453	3451	102	3255	3666	411	27	33.9
U								
V	110	105	17	93	176	83	27	6.6
Zn	85	87	4	75	93	18	27	19.1
Zr	165	164	10	144	182	38	27	17.2

STD	SiO2	SiO2	SiO2	SiO2	SiO2	SiO2	SiO2	SiO2
ppm	Middle	Median	Std	Min	Max	Range	N	Mean/Std
Al								
As								
Ba								
Bal	610255	610221	5961	600200	619182	18982	26	102.4
Ca								
Cl	11305	418	35030	214	166415	166201	27	0.3
Co								
Cr								
Cu								
Fe								
K								
Mn								
Mo								
Nb								
Ni								
P								
Pb								
Rb								
S								
Se								
Si	383430	386623	18002	309033	398469	89436	26	21.3
Sr								
Th								
Ti								
U								
V								
Zn								
Zr								

STD	180-646	180-646	180-646	180-646	180-646	180-646	180-646	180-646
ppm	Middle	Median	Std	Min	Max	Range	N	Mean/Std
Al	47104	47490	2430	43118	51969	8852	27	19.4
As	103	103	3	98	108	10	27	38.3
Ba	474	471	29	408	541	133	27	16.3
Bal	625147	622675	10118	607863	643980	36117	27	61.8
Ca	7205	7182	143	6787	7528	741	27	50.4
Cl	187	180	72	70	338	267	21	2.6
Co	215	214	59	111	345	234	21	3.7
Cr	79	76	11	63	105	42	25	7.2
Cu	222	223	10	198	242	44	27	23.0
Fe	39430	39450	208	39084	39945	861	27	189.1
K	22184	22234	232	21646	22727	1081	27	95.5
Mn	410	415	36	344	477	134	27	11.5
Mo	20	20	2	16	26	10	27	8.4
Nb	14	14	1	13	15	2	27	24.6
Ni	30	30	6	19	42	23	22	4.9
P	1167	1177	117	949	1354	405	27	9.9
Pb	53	53	3	43	58	15	27	15.8
Rb	159	159	2	155	164	9	27	74.1
S	1686	1623	197	1392	2181	789	27	8.6
Se	4	4	1	3	6	3	20	5.4
Si	246030	247901	6602	233436	257216	23780	27	37.3
Sr	110	110	2	106	114	8	27	60.9
Th	49	48	2	45	51	6	27	30.6
Ti	4572	4581	68	4397	4718	321	27	67.2
U								
V	100	95	18	75	153	77	27	5.5
Zn	57	56	5	51	69	19	27	12.1
Zr	403	404	15	364	422	58	27	27.6

Appendix B

HH-XRF data set –available digital from GEUS dataverse (https://doi.org/10.22008/FK2/VXB-PHS) .